Paull, C.K., Matsumoto, R., Wallace, P.J., et al., 1996
Proceedings of the Ocean Drilling Program, Initial Reports, Vol. 164

8. SITE 996[1]

Shipboard Scientific Party[2]

HOLE 996A

Position: 32°29.633′N, 76°11.454′W

Start hole: 0545 hr, 3 December 1995

End hole: 1715 hr, 4 December 1995

Time on hole: 20.75 hr (0.86 days)

Seafloor (drill pipe measurement from rig floor, mbrf): 2181.0

Total depth (drill pipe measurement from rig floor mbrf): 3494.4

Distance between rig floor and sea level (m): 11.4

Water depth (drill pipe measurement from sea level, m): 2169.6

Penetration (mbsf): 63.0

Coring totals:
Type: APC
Number: 4
Recovered: 16.13 m (67.2%)

Type: XCB
Number: 4
Cored: 38.0 m
Recovered: 0.95 m (2.5%)

Type: PCS
Number: 1
Cored: 1.0 m
Recovered: 0.20 m (20.0%)

Formation:
Subunit IB: 0–0.85 mbsf; late Pleistocene; greenish gray nannofossil-rich aragonitic clayey silt with abundant bivalve shell fragments
Subunit IC: 0.85–63.0 mbsf; late Pleistocene to early Pleistocene; greenish gray nannofossil-bearing and nannofossil-rich clay, both with varying amounts of foraminifers (0%–15%) and diatoms (0%–25%)

HOLE 996B

Position: 32°29.634′N, 76°11.455′W

Start hole: 1715 hr, 4 December 1995

End hole: 1800 hr, 4 December 1995

Time on hole: 0.75 hr (0.03 days)

Seafloor (drill pipe measurement from rig floor, mbrf): 2184.1

Total depth (drill pipe measurement from rig floor, mbrf): 2187.5

Distance between rig floor and sea level (m): 11.4

Water depth (drill pipe measurement from sea level, m): 2172.7

Penetration (mbsf): 3.4

Coring totals:
Type: APC
Number: 1
Cored: 3.4 m
Recovered: 3.40 m (100.0%)

Formation:
Subunit IB: 0–1.97 mbsf; age not determined; greenish gray nannofossil-rich aragonitic clayey silt with abundant bivalve shell fragments
Subunit IC: 1.97–3.4 mbsf; age not determined; greenish gray nannofossil-bearing and nannofossil-rich clay, both with varying amounts of foraminifers (0%–15%) and diatoms (0%–25%); carbonate concretions

HOLE 996C

Position: 32°29.638′N, 76°11.455′W

Start hole: 1855 hr, 4 December 1995

End hole: 0200 hr, 5 December 1995

Time on hole: 8.0 hr (0.33 days)

Seafloor (drill pipe measurement from rig floor, mbrf): 2182.1

Total depth (drill pipe measurement from rig floor, mbrf): 2184.7

Distance between rig floor and sea level (m): 11.4

Water depth (drill pipe measurement from sea level, m): 2170.7

Penetration (mbsf): 2.6

Coring totals:
Type: APC
Number: 2
Cored: 2.6 m
Recovered: 2.61 m (100.4%)

Formation:
Subunit IB: 0–0.95 mbsf; age not determined; greenish gray nannofossil-rich aragonitic clayey silt with abundant bivalve shell fragments
Subunit IC: 0.95–2.6 mbsf; age not determined; greenish gray nannofossil-bearing and nannofossil-rich clay, both with varying amounts of foraminifers (0%–15%) and diatoms (0%–25%); carbonate concretions

HOLE 996D

Position: 32°29.634′N, 76°11.478′W

Start hole: 0725 hr, 5 December 1995

End hole: 1545 hr, 5 December 1995

Time on hole: 13.75 hr (0.57 days)

Seafloor (drill pipe measurement from rig floor, mbrf): 2181.0

Total depth (drill pipe measurement from rig floor, mbrf): 2233.2

Distance between rig floor and sea level (m): 11.4

Water depth (drill pipe measurement from sea level, m): 2169.6

---

[1] Paull, C.K., Matsumoto, R., Wallace, P.J., et al., 1996. *Proc. ODP, Init. Repts.,* 164: College Station, TX (Ocean Drilling Program).

[2] Shipboard Scientific Party is given in the list of participants that precedes the Table of Contents.

Penetration (mbsf): 52.2

Coring totals:

Type: APC
Number: 3
Cored: 22.5 m
Recovered: 15.43 m (68.6%)

Type: XCB
Number: 3
Cored: 28.7 m
Recovered: 0.45 m (1.6%)

Type: PCS
Number: 1
Cored: 1.0 m
Recovered: 0.00 m (0.0%)

Formation:

0–22.6 mbsf: very poor recovery of carbonate concretions

Subunit IC: 22.6–52.2 mbsf; late Pleistocene to early Pleistocene; greenish gray nannofossil-bearing and nannofossil-rich clay, both with varying amounts of foraminifers (0%–15%) and diatoms (0%–25%); carbonate concretions

HOLE 996E

Position: 32°29.632′N, 76°11.428′W

Start hole: 1620 hr, 5 December 1995

End hole: 0800 hr, 6 December 1995

Time on hole: 16.25 hr (0.68 days)

Seafloor (drill pipe measurement from rig floor, mbrf): 2181.4

Total depth (drill pipe measurement from rig floor, mbrf): 2243.7

Distance between rig floor and sea level (m): 11.4

Water depth (drill pipe measurement from sea level, m): 2170.0

Penetration (mbsf): 62.3

Coring totals:

Type: APC
Number: 5
Cored: 42.1 m
Recovered: 34.53 m (82.0%)

Type: XCB
Number: 2
Cored: 19.2 m
Recovered: 9.96 m (51.9%)

Type: PCS
Number: 1
Cored: 1.0 m
Recovered: 0.00 m (0.0%)

Formation:

Subunit IA: 0–0.07 mbsf; Holocene(?); brown nannofossil-bearing silty clay

Subunit IC: 0.07–62.3 mbsf; Holocene(?) to early Pleistocene; greenish gray nannofossil-bearing and nannofossil-rich clay, both with varying amounts of foraminifers (0%–15%) and diatoms (0%–25%); carbonate concretions

Principal results: Site 996 is located on the crest of the Blake Ridge Diapir, the southernmost diapir in a series of ~20 diapiric structures rising from deep within the Carolina Trough. The objective at this site was to investigate (1) methane migration and gas hydrate formation in a pockmarked fault zone where methane is leaking out of the continental rise, (2) the source of fluids and gases in a seafloor seep, and (3) the influence of these fluids on the host sediments.

Five short holes were drilled at Site 996 in sediments overlying the Blake Ridge Diapir. Holes 996A, 996B, and 996C are located within a seafloor pockmark that contains an active chemosynthetic community dominated by mussels. Holes 996D and 996E were drilled on the flanks of this pockmark. Overall core recovery was poor. The sedimentary sequence consists primarily of greenish gray nannofossil-bearing clay and nannofossil-rich clay, both with varying amounts of foraminifers (0%–15%) and diatoms (0%–25%). Contorted and steeply dipping beds in parts of the sequence provide evidence of soft-sediment deformation, which was probably caused by slumping and/or faulting related to diapir uplift. The uppermost 2 m of sediment within the pockmark consists of greenish gray nannofossil-rich aragonitic clayey silt with abundant bivalve shell fragments. The shell fragments and surrounding sediments commonly show initial stages of calcite and aragonite cementation. Indurated carbonate zones occur from ~5 to 15 mbsf and from 30 to 50 mbsf. Rapid decreases in the Ca and Mg concentrations of interstitial waters within the upper 10 mbsf and a corresponding increase in the alkalinity indicate the precipitation of carbonate within the uppermost sediments.

All of the sediments recovered at Site 996 are Quaternary in age. The lowermost cores from Holes 996A, 996D, and 996E are early Pleistocene, with a maximum age of ~1.1 Ma. Because of poor recovery, the magnetostratigraphy is very poorly defined. In Hole 996E, the Matuyama/Brunhes boundary is tentatively placed at ~33 mbsf, and the top of the Jaramillo subchron at ~40 mbsf.

Gas hydrate was recovered from all five holes (996A, 996B, 996C, 996D, and 996E). The hydrate was white and occurred in three different forms: (1) massive pieces, cylindrical to round in shape and as much as 5–8 cm long, in sediments recovered from the uppermost 9 mbsf; (2) platy, 1- to 4-mm-thick veins that filled wavy vertical fractures; and (3) vertically oriented rod-shaped nodules ~1 cm in diameter and 3–12 cm long that tapered downcore. Numerous hydrates were sampled both for shipboard analyses and for storage in pressure vessels for shore-based studies. Pieces of hydrate that were too small to be preserved or analyzed were tasted while still fresh by members of the shipboard scientific party.

Magnetic susceptibility and rock-magnetic studies suggest that the zone of bacterial magnetite authigenesis, present in the uppermost few meters at all other Leg 164 sites, is absent from Site 996. High-resolution GRAPE data for sediments from Hole 996E indicate little variation in wet bulk density with depth, with values averaging 1.8 g/cm^3. Porosities decrease from 75% to 50% in the uppermost 12 m of the hole, but water contents decrease exponentially throughout the same interval, similar to the pattern observed in the uppermost 100 m at Sites 994, 995, and 997.

The methane (C_1) contents of headspace gases in sediments from Holes 996A, 996C, and 996D increase from 1300 to 11,000 ppm with increasing depth to 60 mbsf. Ethane (C_2) concentrations ranged from 1 to 10 ppm, yielding C_1/C_2 ratios near 1000. In contrast, near-surface sediments from Hole 996E, which is located outside of the pockmark, were relatively low in C_1. However, at depths below ~10 mbsf, C_1 concentrations and C_1/C_2 ratios were comparable to those from Holes 996A, 996B, and 996C. The free gases were composed of C_1 (more than 90%), CO_2, and H_2S in the upper sections from each hole. H_2S concentrations were as high as 50,000 ppm. Maximum values for C_2 and C_3 were 940 and 25 ppm, respectively.

Chloride concentrations increase to 1.8 times that of seawater with increasing depth (57.7 mbsf) at Site 996, suggesting the influence of evaporites at depth. Increasing Na/Cl ratios and a twofold increase in K^+ concentrations are consistent with a salt source. Large (20%–30%) negative anomalies in chloride concentration also occur, probably because of gas hydrate dissociation.

Sulfate concentrations approach 0 mM near the seafloor (Holes 996C and 996D) and, together with high levels of dissolved ΣHS^- and methane, suggest active sulfate and methane consumption near the seafloor. Active pore-water advection also is suggested by the chemical composition of interstitial waters sampled immediately below the seafloor chemosynthetic community (Holes 996A, 996B, and 996C) and sampled at depth in Hole 996E.

BACKGROUND AND OBJECTIVES

Site 996 is located over the crest of the Blake Ridge Diapir (Fig. 1) on the uppermost portion of the Blake Ridge (see Fig. 2, "Site 994" chapter, this volume). The Blake Ridge is a large sediment drift deposited by the Western Boundary Undercurrent (Tucholke and Mountain, 1979). The diapir is the southernmost in a series of ~20 diapiric structures that rise out of the base of the Carolina Trough along its seaward side (Dillon et al., 1982; Hutchinson et al., 1982). Sites 991, 992, and 993 are located on the next major diapir (Cape Fear Diapir) to the north along the same linear chain of diapirs (see Fig. 1, "Sites 991/992/993" chapter, this volume). The diapirs penetrate a thick sequence of Mesozoic strata into the Tertiary continental rise prism.

The Blake Ridge Diapir is surrounded by an area displaying a strong BSR (Paull and Dillon, 1981). The regional BSR is observed to curve upward around the flanks of the diapir (Figs. 2, 3). The cause of this curvature in the BSR flow is unclear, although it may be related to changes in gas hydrate stability induced by increased heat around the flanks of the diapir. In addition, if the diapir is composed of salt, then the interstitial waters of the overlying sediments may have increased salt contents that would destabilize gas hydrate relative to the surrounding regions, thus causing the BSR to curve upward.

Seafloor venting of microbial gases occurs at 2167 m water depth on the top of the Blake Ridge Diapir (Paull et al., 1995). Acoustically identified, gas-rich plumes extend as much as 320 m above a pockmarked seafloor displaying active chemosynthetic communities. These plumes may be caused by gas bubbles or buoyant clumps of gas hydrate that float upward from the seafloor (Paull et al., 1995).

The plumes apparently emanate from a seafloor pockmark (Figs. 4, 5) that lies along a fault (Fig. 6) that extends downward toward a dome in the BSR (Fig. 2). Side-scan sonar data show that the seafloor along this trace of this fault zone is comparatively reflective. Photographic surveys (Fig. 7) and sampling indicate that these reflective patches are associated with biological communities and methane-derived carbonate cements (Paull et al., 1995), indicating that fluid and/or gas migration is associated with gas hydrate–bearing sediments below.

The objective at this site was to investigate methane migration and gas hydrate formation in a fault zone where methane, presumably derived from the gas hydrate below, is leaking out of the rise. This site offers the potential to establish the influences of these fluids on the host sediments and to investigate the nature of the plumbing below. The source of the fluids and gases in these seafloor seeps may be the gas that is associated with the BSR. We infer that the gas and fluid migrate upward along the flanks of the dome and leak out at the seafloor along the fault plane.

Although this seepage site is active today, numerous small faults are observed to be associated with gas hydrate–bearing zones elsewhere on the continental rise in areas of active seepage (Rowe and Gettrust, 1993). Many of these faults may be sites of former seepages. The potential association of the oceanic gas hydrate reservoir with climatic change requires that there be a dynamic connection between the geologic reservoirs and the atmosphere (Paull et al., 1991). Because gas hydrate is pressure sensitive, the base of the gas hydrate stability zone is likely to have risen during sea-level lowstands, increasing the amount of gas that is available to be vented onto the seafloor. Chemosynthetic communities and authigenic carbonates on and near the seafloor leave a record of venting activity. Comparisons of the volumes of these deposits can help us assess whether the venting has changed with sea-level position and, thus, climate.

Hydrogen sulfide has been noted in piston cores from the crest of the Blake Ridge Diapir (Paull et al., 1995), although no significant amounts H_2S are characteristic of the sedimentary sequences elsewhere in the Blake Ridge area. The setting of Site 996 is very similar to Site 892 (Leg 146) on the Cascadia Margin (Shipboard Scientific Party, 1994) in that both holes were located to intersect a fault plane where active fluid venting occurs. Significant amounts of H_2S occurred in the upper two cores from Site 892, but not at greater depth. The H_2S in both settings may be produced by anaerobic methane oxidation (Reeburgh, 1982) in which venting methane mixes with seawater sulfate within the seafloor. A primary objective of drilling at Site 996 was to test this hypothesis.

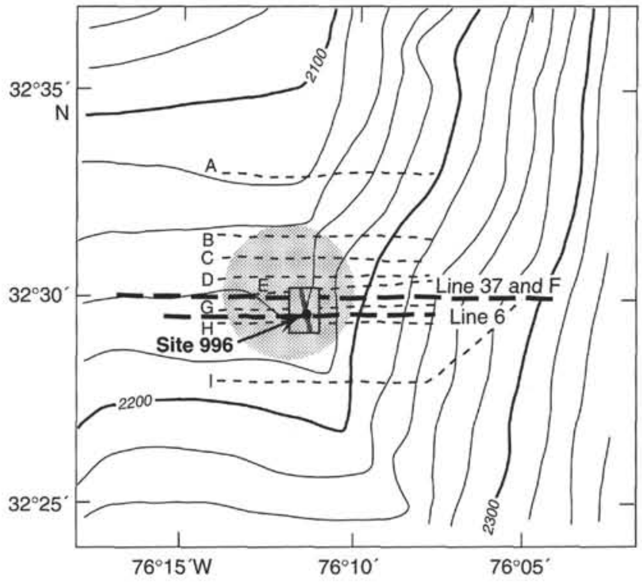

Figure 1. Bathymetry over the Blake Ridge Diapir with respect to Site 996. The area where the diapir occurs in the subsurface is schematically indicated with the large shaded circle. The location of CH-06-92 Line 37 (Fig. 2), which passes near Site 996, and *JOIDES Resolution* Line 6, which crosses over Site 996 (Fig. 3), are indicated by the bold dashed lines. The trace of the small north-northwest–south-southeast trending fault, along which Site 996 was located, is indicated by a short hatched line through the drill site. The location of side-scan sonar data, shown in Figure 4, is illustrated with the small box. The location of the 3.5-kHz profiles A through I (illustrated in Fig. 6) are shown with the finer dashed lines. Contours are in meters.

The pockmark that occurs at Site 996 and those that occur at many other seafloor seeps (Hovland and Judd, 1988; Matsumoto, 1990) are clearly related to seafloor methane seepage. However, the actual mechanism of pockmark formation is unclear. It has been suggested that these pockmarks are created where massive gas hydrate forms at the seafloor along the fault (Paull et al., 1995). Because the density of gas hydrate is only 0.910 g/cm^3 at 0°C (Davidson et al., 1983), when gas hydrate occupies more than 90% of the host sediments, the affected sediment mass will be less dense than seawater. Elsewhere, clumps of gas hydrate have been observed to break loose from the bottom and float upward (MacDonald et al., 1994). Thus, it is hypothesized that clumps of sediment may be rafted out of the pockmarks and drift downstream in the current. Bottom photographs at this site indicate that there are dropstone-like blocks of carbonate-cemented strata (Fig. 7D) that are scattered on the seafloor downstream of the pockmark (Paull et al., 1995).

OPERATIONS

Transit to Site 996

A 72-km transit was completed in 3.2 hr at 12.2 kt, and a 63-km seismic survey was conducted over Site 996 (proposed site BRD-1) in 4.8 hr at 7.0 kt. A Datasonics 354M beacon was dropped on Global

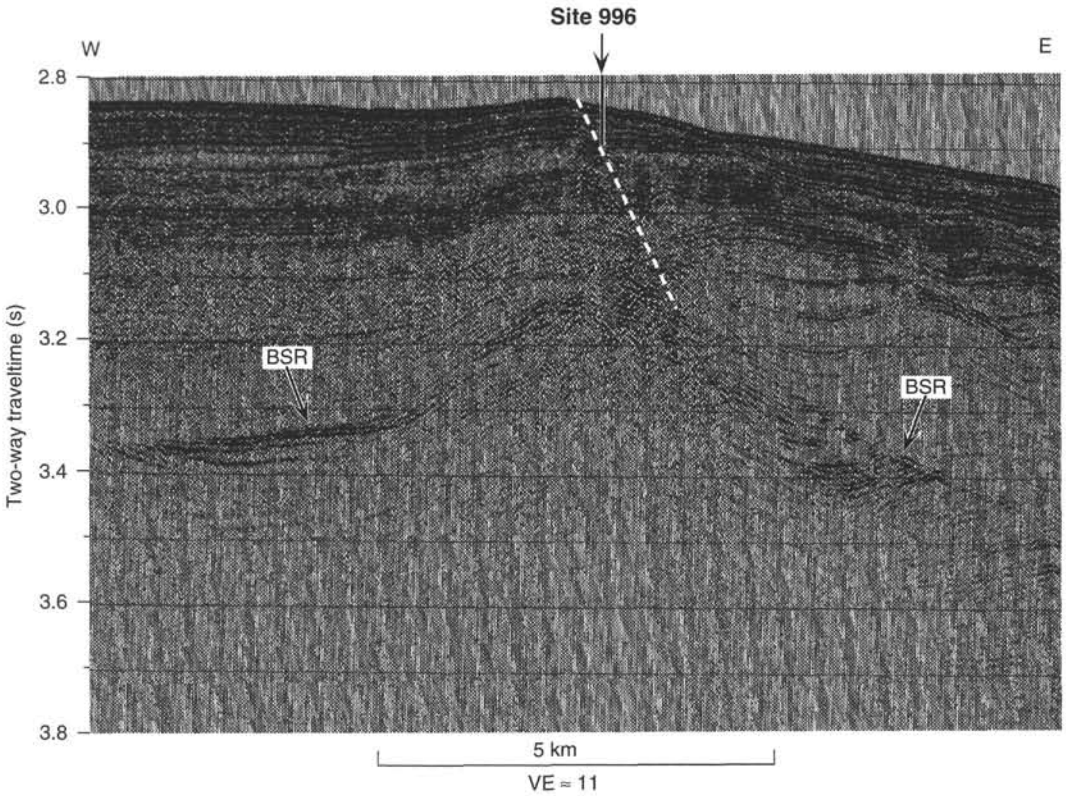

Figure 2. Seismic Profile CH-06-92 Line 37 immediately north of Site 996. The fault along which venting is occurring is indicated with a dashed line.

Positioning System (GPS) coordinates 32°29.629′N, 76°11.480′S. The same APC/XCB drill string was run with a flapper valve and without a monel drill collar. The vibration-isolated television (VIT) frame was run with a television (TV) camera, sonar, a VIT frame beacon, and a deployable beacon. A TV and sonar survey was run from 150 m west to 70 m east of the GPS coordinates at the point where the beacon was dropped. Accurate navigation during the survey was ensured by the use of differential GPS (see "Operations" section, "Sites 991/992/993" chapter, this volume). Carbonate crusts were evident over most of the transect, and a bed of chemosynthetic mussels was located between 30 and 50 m east of the GPS coordinates. Cross surveys indicated that this mussel bed extended at least 10 m to the north and south. The seafloor was tagged with the bit at 2169.6 m below sea level (mbsl) water depth, and the bit was positioned in the center of the mussel bed.

Hole 996A

Hole 996A was spudded at 0545 hr on 4 December (Table 1). The first APC core shot was observed with the TV camera, and the seafloor was at 2169.6 m water depth. Cores 164-996A-1H and 2H were taken from 0 to 9.5 mbsf. Core 164-996A-2H was a partial stroke that hit a hard carbonate. The VIT frame was pulled to permit rotation with the XCB coring system. Cores 164-996A-3X through 6X were taken from 9.5 to 47.5 mbsf. Coring parameters indicated a soft matrix with a hard crust from 10 to 15 mbsf and from 28 to 30 mbsf. The last three XCB cores had no recovery. Core 164-996A-7P was taken from 47.5 to 48.5 mbsf and was recovered with an internal pressure of 3326 psi. Cores 164-996A-8H and 9H were taken from 48.5 to 63.0 mbsf. Verbal approval was obtained from ODP to obtain cores from 50 to 63 mbsf to obtain more hydrate. H_2S was noted in Cores 164-996A-1H and 2H, with concentrations of 60 to more than 100 ppm (maximum detector range). Gas masks were used, and entry to the catwalk area was restricted. A fan was used to blow gas out of the area. Cores were sectioned, holes were drilled in the liners, and the cores were laid on the grating of the catwalk to degas. Most cores degassed within 30 min, but some cores required more than 2 hr to reach less than 10 ppm H_2S. Some core liners were cut in the lab and carried outside to be split and opened for degassing. As a result of the H_2S gas, hydrate could not be readily sampled in the upper cores.

Hole 996B

The ship was not moved, and Hole 996B was spudded at 1735 hr on 4 December in an effort to obtain near-surface sediments for shore-based microbiological studies. The bit was positioned at 2166.6 mbsl (3 m higher than on Hole 996A) for Core 164-996B-1H, but the core was blown apart in the liner and the sediment blew out on the deck. Recovery was 3.4 m.

Hole 996C

The ship was not moved, and Hole 996C was spudded at 1855 hr on 4 December in an effort to obtain more near-surface sediments. The bit was positioned at 2163.6 m (6 m higher than on Hole 996A), and Core 164-996C-1H recovered a mudline with 2.4 m recovered. Core 164-996C-2H was an incomplete stroke. The core barrel could not be retrieved after 2.5 hr, so the drill string was pulled. The core barrel had been bent by the impact with a hard layer (probably carbonates) within 2.6 m of the surface.

Hole 996D

While running in with the same BHA, the ship was moved 40 m west. Hole 996D was spudded at 0725 hr on 5 December. The seafloor was estimated at 2169.1 mbsl, based on an apparent seafloor

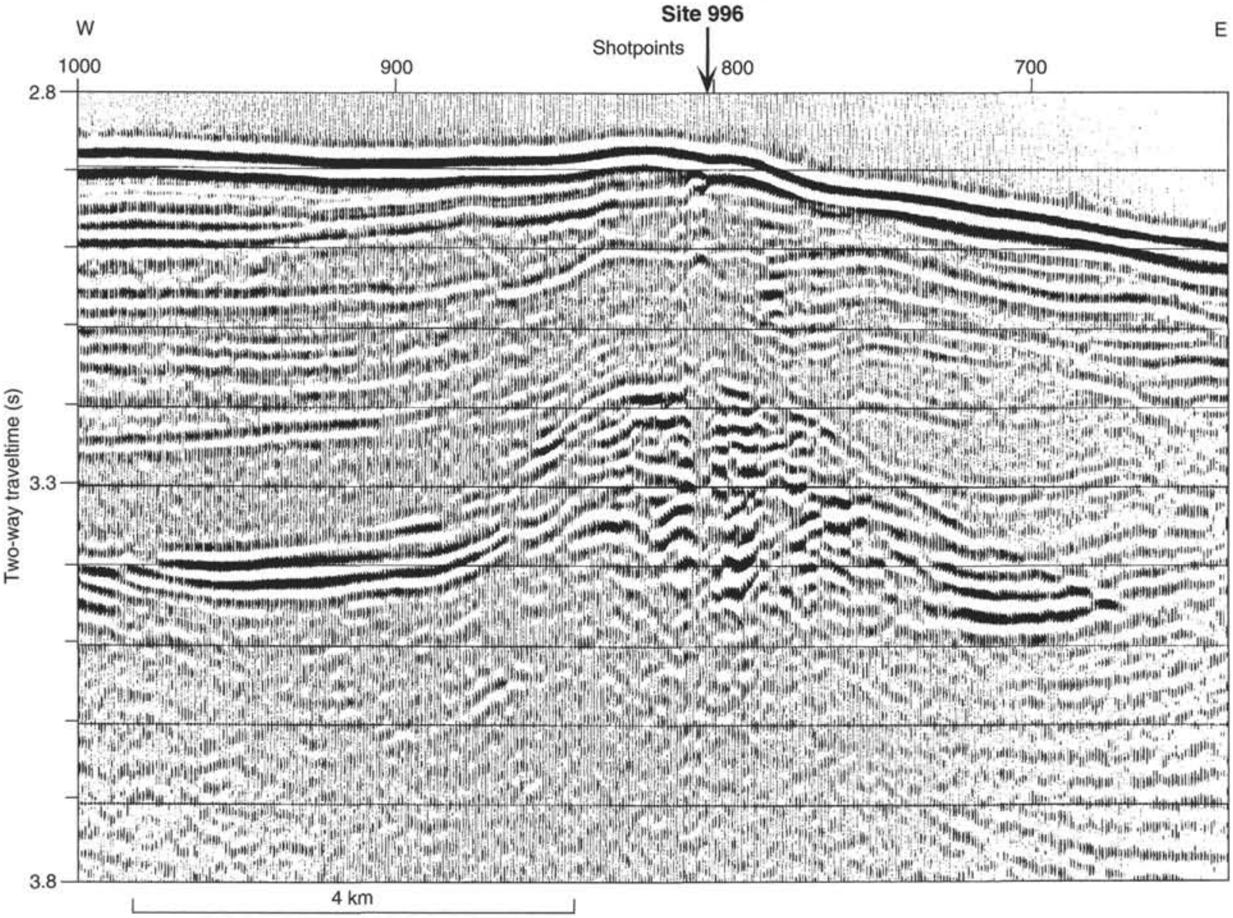

Figure 3. Seismic reflection profile (Line 6) across Site 996 collected from the *JOIDES Resolution* during Leg 164.

penetration of 3.5 m into a hard crust. Core had apparently fallen out of the core barrel because actual recovery on Core 164-996D-1H from 0 to 3.5 mbsf was only 0.40 m. The core barrel was bent and had a broken shoe section. The XCB coring system was picked up, and Cores 164-996D-2X and 3X were taken from 3.5 to 22.6 mbsf, with 1% recovery. Coring parameters indicated a soft matrix with a moderately hard crust from 13 to 14 mbsf and from 17 to 19 mbsf. Core 164-996D-4H from 22.6 to 32.1 mbsf had 92% recovery, but the overpull was 60,000 lb, with a hard carbonate layer at 29–32 mbsf. Core 164-996D-5X was taken from 32.1 to 41.7 mbsf, with 3% recovery. Core 164-996D-6H was taken from 41.7 to 51.2 mbsf, and Core 164-996D-7P was taken from 51.2 to 52.2 mbsf. It was recovered at 2974 psi (91% of hydrostatic pressure at the recovery depth) but contained no sediment.

Hole 996E

The ship was moved 80 m east of Hole 996D, and Hole 996E was spudded at 0725 hr on 5 December. The seafloor was estimated at 2170.0 mbsl, based on recovery of a mudline. Cores 164-996E-1H and 2H were taken from 0 to 13.6 mbsf in a soft matrix and bottomed out in a hard crust. Core 164-996E-3X was taken from 13.6 to 23.2 mbsf in the hard crust. Cores 164-996E-4H and 5H were taken from 23.2 and 42.2 mbsf in a soft matrix. Core 164-996E-6X was taken from 42.2 to 51.8 mbsf in a hard crust. A final APC core (164-996E-7H) was taken from 51.8 to 61.3 mbsf in a soft matrix, and Core 164-996E-8P was taken from 61.3 to 62.3 mbsf. It was recovered at 944 psi (29% hydrostatic) but contained no core. The PCS actuator was found to be sanded up. The drill string was pulled and inspected on the way out. The beacon-recall sender unit in the hull was found to be defective, and both beacons were recalled with the portable unit and recovered. This could explain the two beacon-recall failures earlier in the leg.

LITHOSTRATIGRAPHY

Introduction

Five holes were drilled at Site 996 in sediments overlying the Blake Ridge Diapir. Holes 996A, 996B, and 996C are located beneath an active chemosynthetic community (Fig. 8). Holes 996D and 996E were drilled on the flanks of this community, ~40 m to the west and east of Holes 996A, 996B, and 996C (Fig. 9). Core recovery in Holes 996A, 996B, 996C, and 996D was poor (see Figs. 9, 20), and the following lithostratigraphic description is based on a combination of observations from all five holes. One lithologic unit, divided into three subunits, is recognized.

Unit I

Intervals: 164-996A-1H-1 through 9H-CC; 164-996B-1H-1 through 1H-CC; 164-996C-1H-1 through 2H-CC; 164-996D-1H-1 through 6H-CC; 164-996E-1H-1 through 7H-CC
Age: early Pleistocene to Holocene
Depth: 0–63.00 mbsf

Unit I consists predominantly of greenish gray to gray (5GY 5/1 to 5G 6/1 and 5Y 5/1) nannofossil-bearing silty clay and nannofossil-rich clay with varying amounts of foraminifers and diatoms. Carbon-

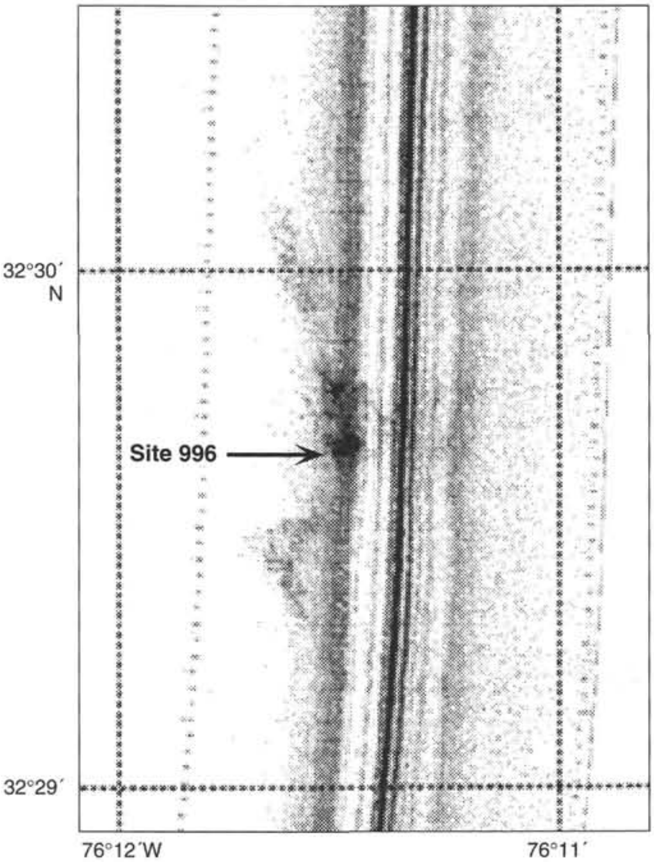

Figure 4. A slant range corrected side-scan sonar profile showing seafloor reflectivity in the vicinity of Site 996. The area covered is indicated in Figure 1. Data were collected with the Scripps Institution of Oceanography's deep-tow system during *Knorr* research cruise 140-1. Darker shades are more reflective. The arrow indicates the pockmark targeted at Site 996.

ate concretions found at various depths throughout Unit I (Table 2) are classified as calcirudites and biocalcirudites (Fig. 10). The different types of lithified carbonates are described below.

Unit I is divided into Subunits IA, IB, and IC. Subunit IA is a distinctive, thin brownish section at the top of the unit in Hole 996E. Subunit IB consists primarily of thick beds of partially cemented shell fragments and surrounding sediment. These beds are as much as 2 m thick and form the top of Holes 996A, 996B, and 996C, which are located beneath the biological community (Fig. 9). Subunit IC is composed of nannofossil-bearing silty clay with varying foraminifer and diatom abundances. This subunit is present in all five holes.

Subunit IA

Subunit IA (interval 164-996E-1H, 0–7 cm; 0–0.07 mbsf) consists of brown (10YR 5/3), bioturbated nannofossil-bearing silty clay and is equivalent to Subunit IA at Sites 994, 995, and 997 (e.g., Fig. 8, "Lithostratigraphy" section, "Site 994" chapter). This subunit is present only in Hole 996E. The base of Subunit IA in Hole 996E is marked by a gradual transition from Subunit IA to IC; Subunit IB is absent. This transition is characterized by an 8-cm-thick band with gradational colors from brown to gray (5Y 6/1) (interval 995-1H-1, 7–15 cm; 0.07–0.15 mbsf).

Subunit IB

Subunit IB extends from 0 to 0.85 mbsf in Hole 996A (interval 164-996A-1H-1, 0–85 cm); from 0 to 1.97 mbsf in Hole 996B (interval 164-996B-1H-1, 0 cm, through 1H-2, 105 cm); and from 0 to 0.95 mbsf in Hole 996C (interval 164-996C-1H-1, 0–95 cm). This subunit consists of greenish gray to gray (5GY 5/1 to 5Y 5/1) nannofossil-rich aragonitic clayey silt with abundant bivalve shells and carbonate nodules. Most of the bivalve shells are broken into fragments 1–5 cm in size, and they comprise as much as 50% of the total sediment volume. The shell fragments and surrounding sediments commonly show initial stages of carbonate cementation. Silt-sized aragonite needles are very abundant in the surrounding sediment but become less abundant downhole. Much of the original sediment texture was destroyed during the coring process because of the poorly consolidated nature of the sediment. Subunit IB is absent in Holes 996D and 996E because these holes were drilled outside of the region occupied by the living bivalve communities (Fig. 9).

Subunit IC

In Holes 996A, 996B, and 996C, the top of Subunit IC is defined as the first bivalve shell–free sediment immediately beneath the lowermost occurrence of sediments dominated by shell fragments, which characterize Subunit IB (164-996A-1H-1, 85 cm; 164-996B-1H-2, 105 cm; and 164-996C-1H-1, 105 cm; 0.85, 1.97, and 1.05 mbsf, respectively) (Fig. 9). Because Subunit IB is missing in Hole 996E, the top of Subunit IC is placed at 0.07 mbsf (164-996E-1H-1, 7 cm), below the base of Subunit IA. The boundary of Subunit IC is uncertain in Hole 996D because no sediment was recovered above 22.60 mbsf. Subunit IC extends to the bottom of all holes at Site 996.

Lithologic description of Subunit IC is primarily based on sediments recovered in Hole 996E because of the relatively high sediment recovery (Figs. 9, 20). The sediment consists of greenish gray to gray (5GY 5/1 to 5G 6/1) nannofossil-bearing silty clay and nannofossil-rich clay with varying abundances of foraminifers and diatoms. Solid gas hydrate was recovered from various intervals of this subunit. Detailed description of the gas hydrate occurrences is given in the "Gas Hydrate" section (this chapter).

Sediment intervals 164-996E-2H-1, 81–125 cm (4.91–5.35 mbsf), and 2H-3, 10–73 cm (7.20–7.83 mbsf), are clay conglomerates composed of discrete clay clasts of various sizes and shapes showing variegated shades of greenish gray to gray (5GY 5/1 to 5Y 6/1) colors. Clasts are round to angular in shape and commonly show evidence of soft-sediment deformation (Fig. 11 and the whole-core photograph in Section 4, this volume). Abrupt changes in lithology and color, contorted and steeply dipping beds, and the presence of clay clasts all suggest that soft-sediment deformation has occurred.

Authigenic Carbonate Concretions

Authigenic carbonate concretions were recovered from various depths in Holes 996A, 996B, 996C, 996D, and 996E (Table 2). Zones of poorest sediment recovery at Site 996 coincided with significant decreases in penetration rates during core cutting (Fig. 12; also see "Operations" section, this chapter). Material recovered from those zones consisted entirely of fragments of indurated carbonate rock.

In Hole 996A, Core 2H was blocked by a hard bed at 9.5 mbsf (see "Operations" section, this chapter) and lithified carbonate concretions were recovered from the core catcher (Table 2). Continued drilling with the XCB resulted in variable penetration rates in the interval from 10 to 48 mbsf (Fig. 12), suggesting alternating indurated and semi-indurated lithologies. Core recovery through this entire zone consisted of one (5 cm in diameter) carbonate nodule from 19.0 mbsf. Penetration rates in Hole 996D were low throughout much of the upper 24 m, and recovery consisted of few carbonate nodules at 3.5, 13.0–13.6, 23.0, and 24.5 mbsf (Table 2). A hard crust was reached at 13.6 mbsf in Hole 996E (see "Operations" section, this chapter). From 13.6 to 23.2 mbsf (Fig. 12), penetration was slow. Poor recovery yielded 35 cm of biocalcirudite and calcirudite nodules. A reduction in penetration at 51.8 mbsf was associated with recovery of carbonate nodules in Core 164-996E-6X at 51.62–51.73 mbsf. The slow

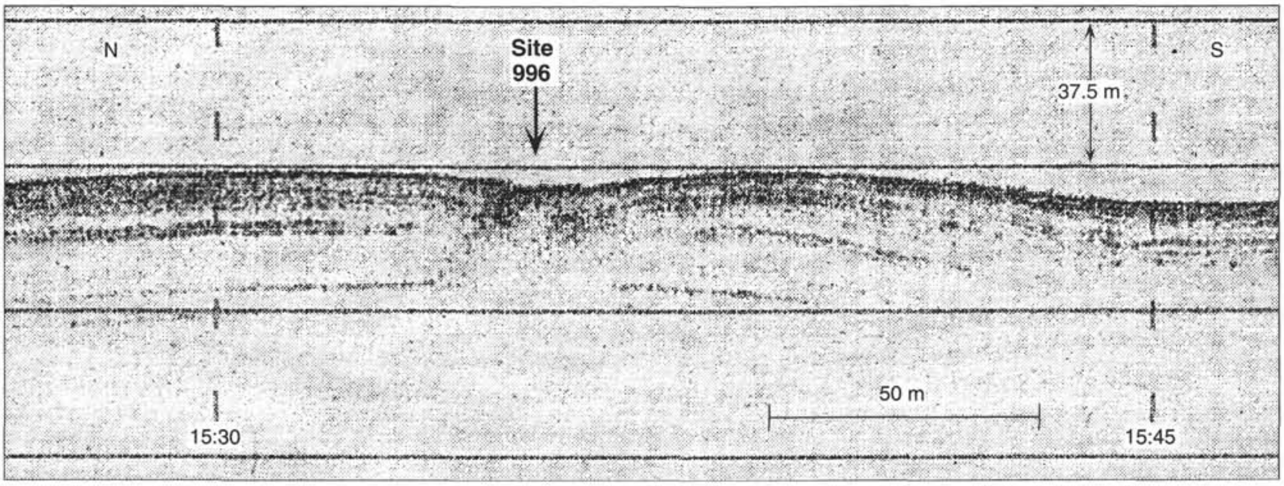

Figure 5. North-south oriented 4.0-kHz profile collected across the pockmark imaged in Figure 4. Data were collected with the Scripps Institution of Oceanography's deep-tow system during *Knorr* research cruise 140-1. The instrument was towed about 100 m off the seafloor.

penetration and very poor recovery in all three holes are suggestive of well-indurated carbonates occurring either in beds, or in patches, within this region.

In hand specimen, two basic types of carbonate concretions can be distinguished: (1) calcirudites (after Carozzi, 1989) that are composed of rounded to subangular intraclasts (0.5–2 cm in size) and (2) biocalcirudites that primarily consist of carbonate-cemented shell fragments (Fig. 10). Intraclasts are predominately grain-supported calcarenites and biocalcarenites (Fig. 13) with a micrite matrix. Foraminifers and bivalve fragments dominate the biogenic components. Silt-sized quartz, feldspar, pyrite, glauconite, and clay are the main clastic and noncarbonate components. The micrite matrix often exhibits a peloidal texture (Fig. 13). The biocalcarenites contain higher amounts of biogenic components, mainly bivalve shells and foraminifers. The terminology used to describe the concretions is based on textural characteristics and does not imply a genetic origin. Following strict adherence to Carozzi's (1989) classification, the characteristics would be considered bioaccumulated limestones.

At least three generations of carbonate cement can be recognized in these rocks in thin section. A microcrystalline interstitial carbonate cement represents the first stage of lithification and characterizes the fabric of the intraclasts contained within the calcirudites. Fibrous aragonite needle cements (filling open pores of bioclasts within the intraclasts) and both radial fibrous aragonite and radiating bladed calcite crystals (filling the pore space between the intraclasts) represent a second stage of lithification. Well-developed radiating crystals of aragonite occur where earlier generations of aragonite do not fill the entire pore space (Fig. 13). Cavity-filling, equant sparite represents a later stage of carbonate cementation. Nodules found within Subunit IB do not exhibit the multiple generation botryoidal aragonite and calcite, or equant sparite cements, that are found in nodules recovered from deeper in the holes as described above.

Sediment Composition Based on Smear-Slide and XRD Analyses

Site 996 sediments have been strongly influenced by diagenesis associated with fluid seepage. Nonetheless, the lithologic character of sediments in the region can be ascertained based on the integration of data from all five holes. The dominant mineral components, excluding the carbonate concretions described above, are clay minerals, calcite, and quartz. Feldspar, dolomite, and aragonite are minor components. Micas, glauconite, and other accessory minerals are present in trace amounts.

Biogenic components include nannofossils, diatoms, foraminifers, and shell fragments. Nannofossils range in abundance from 5% to 40%; foraminifer abundance ranges from 1% to 15%; and shell fragments (as much as 50% of the bulk sediment) are associated with carbonate concretions and the mussel beds at the top of Holes 996A, 996B, and 996C. Higher abundances of foraminifers (12%–15%) occur in interval 164-996A-8H-1, 40 cm, through 9H-6, 150 cm (48.90–63.75 mbsf), and in Sample 164-996E-2H-1, 68 cm (4.78 mbsf). Diatoms are more abundant in Holes 996D and 996E, in interval 164-996D-6H-4, 0 cm, through 6H-5, 100 cm (44.49–46.21 mbsf), and in Sample 164-996E-6X-2, 45 cm (43.96 mbsf). Increases in the nannofossil content coincide with increased diatom abundance.

Quartz content ranges from 5 to 30 wt% (estimated from XRD), and clay-mineral content is essentially constant downhole (Fig. 14; Table 3). Calcite content ranges from 12 to 62 wt% and reflects both the biogenic and authigenic components of these sediments (Fig. 14). Peaks in calcite content (62, 45, and 35 wt%) at 9.80 mbsf (Sample 164-996A-3X-1, 30 cm), 37.78 mbsf (Sample 164-996E-5H-5, 73 cm), and 43.95 mbsf (Sample 996E-6X-2, 45 cm), respectively, correspond to increased nannofossil abundance (as indicated by smear-slide observations). Dolomite content is low throughout much of the sediment column (1–5 wt% from XRD estimates), but peaks in abundance occur in intervals 164-996D-6H-2, 40–41 cm (42.87–42.88 mbsf), and 164-996E-5H-7, 0–72 cm (38.97–39.69 mbsf). The d-spacing of the (104) diffraction peak ranges from 2.887 to 2.909 Å, which is indicative of compositions reflecting both near-stoichiometric and nonstoichiometric dolomite (Table 3). Aragonite content reflects the occurrence of bivalve shell fragments and authigenic aragonite needles in the matrix clays of Subunit IA (60% as estimated by smear-slide observation) and as pore-filling cements within the nodules.

Discussion

Five holes drilled at Site 996 are located on the crest of the Blake Ridge Diapir, a broad topographic high on the seafloor (Fig. 9). The sediments recovered at Site 996 are dominated by a hemipelagic accumulation of biogenic and terrigenous sediments. Sediments on the flanks and crests of diapirs are generally subject to failure because of the steeper slopes associated with these features. Such sediment failure generates localized mass-transport deposits, usually slumps and debris flows. Subunit IC in Hole 996E clearly contains intervals of clay conglomerates (Fig. 11) composed of disturbed sediments that have undergone soft-sediment deformation during failure and subsequent deposition by mass-transport processes (e.g., slumping, slid-

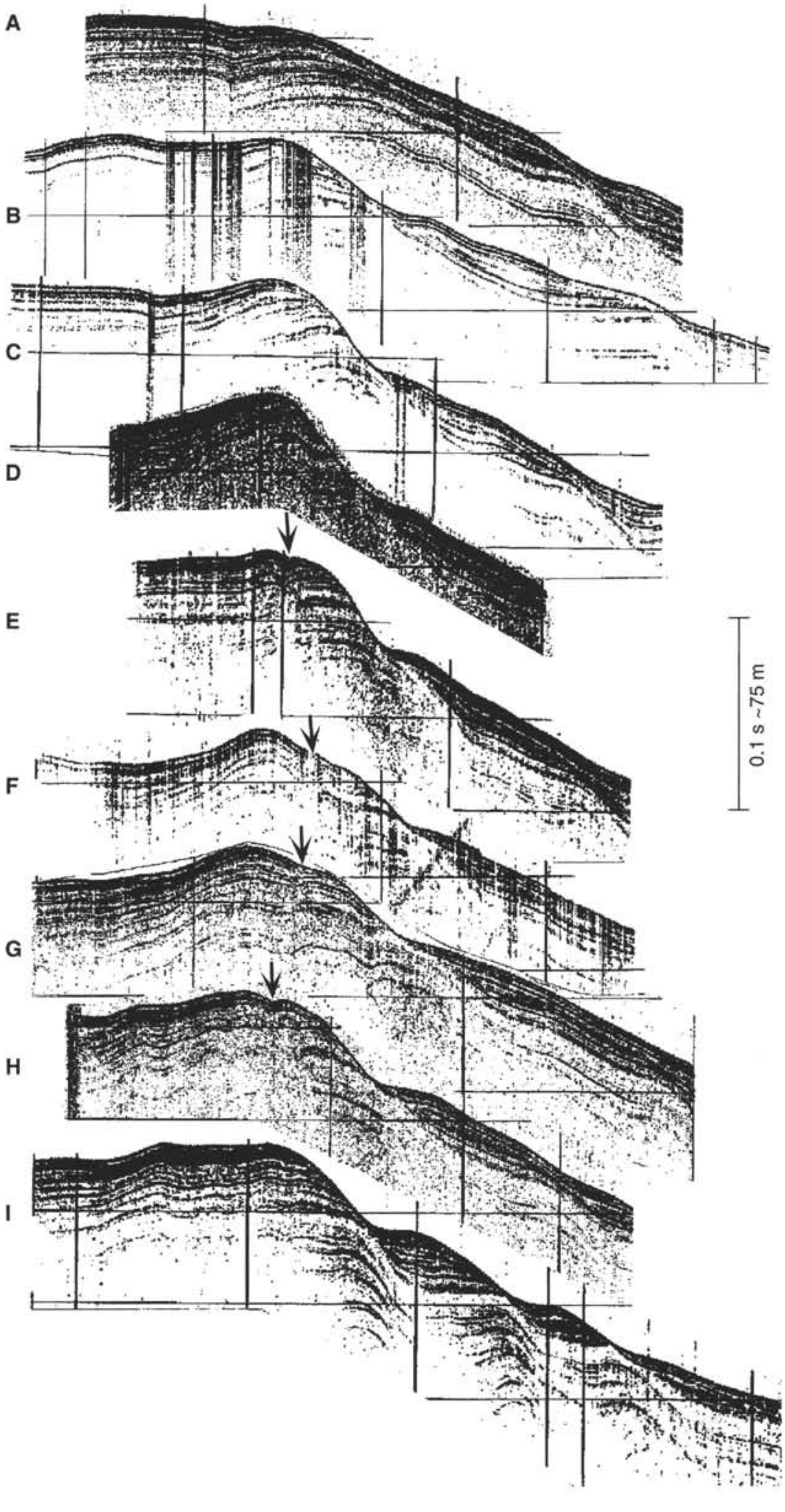

Figure 6. Nine east-west oriented 3.5-kHz profiles, labeled A through I, across the crest of the Blake Ridge Diapir in the vicinity of Site 996. The locations of the profiles are shown in Figure 1. Data were collected during *Cape Hatteras* cruises CH-06-92, CH-11-92, and CH-31-93. Site 996 is located between profiles G and H. Arrows above profiles E, F, G, and H indicate the location of a small fault. The trace of this fault corresponds to the reflective seafloor illustrated in Figure 4. Slide scars are common on the eastern flank of this structure.

ing, and debris flows). Similar mass-transport deposits were recovered at Sites 991 and 992 (see "Lithostratigraphy" section, "Sites 991/992/993" chapter, this volume). However, the thickness of mass-transported deposits at Site 996 is much less than at Sites 991 and 992 and suggests more localized mass-transport events on the flanks of the Blake Ridge Diapir.

Chemosynthetic communities and associated carbonate crusts similar to those observed at Site 996 have been observed at many locations along both active and passive continental margins, in regions where methane-rich fluids are seeping out onto the seafloor (Hovland et al., 1987; Ritger et al., 1987; Matsumoto, 1990; Jorgensen, 1992; Paull et al., 1992, 1995). At Site 996, a small fault extends downward

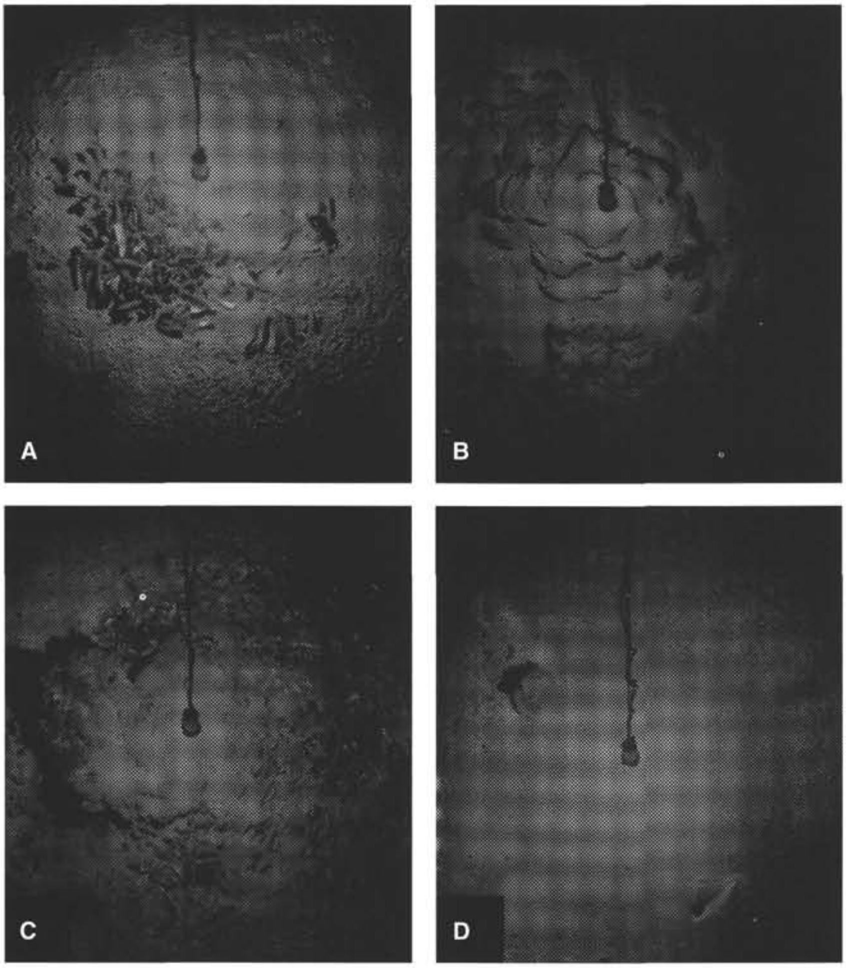

Figure 7. Seafloor photographs taken with the Scripps Institution of Oceanography's deep-tow system near the pockmark illustrated in Figures 4 and 5 during *Knorr* research cruise 140-1. The field of view is about 4 m. **A.** A (chemosynthetic?) mussel bed (~2165 m water depth). **B.** Outcropping rocks that apparently have been exhumed at the edge of the pockmark in ~2166 m of water. These rocks are interpreted to be methane-derived carbonate cements because core samples from near or within this pockmark contain such authigenic cements with light $\delta^{13}C$ (~–40‰ PDB) values (Paull et al., 1995). **C.** The seafloor within a pockmark in ~2,169 m of water containing partly exhumed (methane-derived carbonate?) crusts flanked by beds of living and dead mussels. Many of these mussels are covered with a thin dusting of finer sediment. **D.** An isolated rock sitting on the seafloor, extensive areas of white, textured bottom, and several burrows and mounds on the seafloor in ~2165 m of water. Isolated rocks are common in this area both within and proximal to seafloor pockmarks. One possible origin for such rocks is that they are gas hydrate-rafted dropstones.

through the sediments and shallow BSR over the Blake Ridge Diapir and appears to provide a conduit for venting of microbial gas to the seafloor. These CH_4-rich vent fluids support an active chemosynthetic community and stimulate authigenic carbonate precipitation (Paull et al., 1995). Cementation in the near-surface sediments is likely to be caused by increases in alkalinity associated with microbial sulfate reduction and methane oxidation. The carbonate cements observed at Site 996 resemble cements described at many other seep sites (e.g., Hovland et al., 1987; Ritger et al., 1987; Matsumoto, 1990), and they are characterized by multiple generations of cementation, including microcrystalline replacement of matrix clays, needle and radial fibrous aragonite, radiating bladed calcite cement, and equant pore-filling sparite. The nodules recovered from the uppermost part of the sediment column do not exhibit the multiple stages of cementation observed in nodules recovered from depth. Although multiple generations of cementation could occur on, or within centimeters below, the seafloor (Hovland et al., 1987; Ritger et al., 1987; Matsumoto, 1990), the fact that no extensive cementation in the nodules of Subunit IB was observed suggests that authigenic carbonate precipitation may continue with depth and may be indicative of a complex fluid regime.

Because the fault at Site 996 extends downward through the BSR, it is likely that the fluids from which the carbonate precipitates are derived from the decomposition of gas hydrate in the underlying sediments. As methane from below the BSR passes into the gas hydrate stability zone along the observed fault, gas hydrate should form (Paull et al., 1995). Hydrate formation will influence the porosity and permeability of these near-surface sediments and, thus, alter the normal flow of fluids within the region.

GAS HYDRATE

Gas hydrate was observed in sediments recovered from all five holes drilled at Site 996.

Hole 996A

The location of Site 996A was chosen within a pockmark, based on a VIT camera and sonar survey. The first APC core was shot into a dense mussel bed. The first two cores from Site 996 evolved enough H_2S to set off the H_2S detectors on the drill rig. Breathing apparatuses were used by the people handling the cores. Handheld H_2S meters inserted into the void spaces at the ends of the cores indicated H_2S concentrations of 60 to more than 100 ppm (the limit of the sensors). Thus, the cores were left on the catwalk for more than an hour to degas, and no observations about their gas hydrate concentrations could be made. Because the APC coring system did not fully extend on Core 164-996A-2H, the following cores were cut with the XCB. Core 164-996A-3X still contained 10–40 ppm of H_2S. XCB Cores 164-996A-3X to 6X contained almost no recovery. Core 164-996A-8H was taken with the APC in an attempt to achieve better recovery.

Core 164-996A-8H contained gas hydrate in the core catcher. Several sections of the core had anomalously low temperatures (~2°C). Two sections of this core were split in half. Exposed surfaces revealed veins of white gas hydrate, as much as 0.5 cm thick and 3–4 cm wide, that could be traced ~30–40 cm along the core. The gas hydrate was actively fizzing and disappeared within ~10 min.

Core 164-996A-9H was taken from 58.0 to 63.0 mbsf and, upon recovery, appeared to contain gas hydrate throughout the core. Sec-

Table 1. Coring summary for Site 996.

Core	Date (Dec. 1995)	Time (UTC)	Depth (mbsf)	Length cored (m)	Length recovered (m)	Recovery (%)
164-996A-						
1H	4	1100	0.0–8.5	8.5	4.08	48.0
2H	4	1150	8.5–9.5	1.0	0.69	69.0
3X	4	1530	9.5–19.0	9.5	0.94	9.9
4X	4	1615	19.0–28.5	9.5	0.01	0.1
5X	4	1730	28.5–38.0	9.5	0.00	0.0
6X	4	1830	38.0–47.5	9.5	0.00	0.0
7P	4	1915	47.5–48.5	1.0	0.20	20.0
8H	4	1955	48.5–58.0	9.5	5.43	57.1
9H	4	2120	58.0–63.0	5.0	5.93	118.0
Coring totals				63.0	17.28	27.4
164-996B-						
1H	4	2250	0.0–3.4	3.4	3.40	100.0
Coring totals				3.4	3.40	100.0
164-996C-						
1H	5	0015	0.0–2.4	2.4	2.41	100.0
2H	5	0715	2.4–2.6	0.2	0.20	100.0
Coring totals				2.6	2.61	100.0
164-996D-						
1H	5	1245	0.0–3.5	3.5	0.40	11.4
2X	5	1330	3.5–13.0	9.5	0.01	0.1
3X	5	1530	13.0–22.6	9.6	0.16	1.7
4H	5	1610	22.6–32.1	9.5	8.42	88.6
5X	5	1740	32.1–41.7	9.6	0.28	2.9
6H	5	1815	41.7–51.2	9.5	6.31	66.4
7P	5	1950	51.2–52.2	1.0	0.00	0.0
Coring totals				52.2	15.58	29.8
164-996E-						
1H	5	2135	0.0–4.1	4.1	4.09	99.7
2H	5	2215	4.1–13.6	9.5	9.05	95.2
3X	6	0115	13.6–23.2	9.6	0.36	3.8
4H	6	0150	23.2–32.7	9.5	6.77	71.2
5H	6	0240	32.7–42.2	9.5	7.53	79.2
6X	6	0410	42.2–51.8	9.6	9.60	100.0
7H	6	0445	51.8–61.3	9.5	7.09	74.6
8P	6	0605	61.3–62.3	1.0	0.00	0.0
Coring totals				62.3	44.49	71.4

Notes: UTC = Universal Time Coordinated. An expanded version of this coring summary table that includes lengths and depths of sections and sampling comments is included on CD-ROM in the back pocket of this volume.

tions 164-996A-9H-1 and 2 were cut open immediately. Wavy, approximately vertical veins of gas hydrate, similar to those found in Core 164-996A-8H, were present throughout both sections. It was difficult to determine whether the gas hydrate was a single vein that continued through both sections.

Holes 996B and 996C

The objective of drilling Holes 996B and 996C was to recover good mudline cores in the same area as Hole 996A. Initial measurements with handheld H_2S meters indicated that the H_2S levels exceeded 100 ppm in the air around the cores, so the cores were left outside on the catwalk to degas. Limited catwalk sampling was conducted with the assistance of breathing apparatuses. Several gas hydrate nodules were seen in Cores 164-996B-1H and 2H when they were sectioned for microbiology samples. The largest was a spherical nodule 5 to 6 cm in diameter that was recovered from Section 164-996B-1H-3. The surface of this nodule was opaque, white, and smooth. The nodule was not observed to bubble vigorously. No sediment was adhering to the exterior of the sample. The through-core-liner temperatures of Sections 164-996B-1H-5 and 6 were 6.7° and 8.4°C, respectively.

Core 164-996C-1H also contained dangerous levels of H_2S (>100 ppm), which seriously restricted access to the core. Several pieces of gas hydrate were observed in the core catcher. Two pieces were cylindrical in shape and 5–8 cm in length. One of these appeared to be composed entirely of gas hydrate, with little sediment attached. The other piece was marbled with hydrate and sediment. Hole 996C was terminated unexpectedly after Core 164-996C-2H because the core barrel bent when it struck a hard carbonate bed at ~2.6 mbsf (see "Operations" section, this chapter).

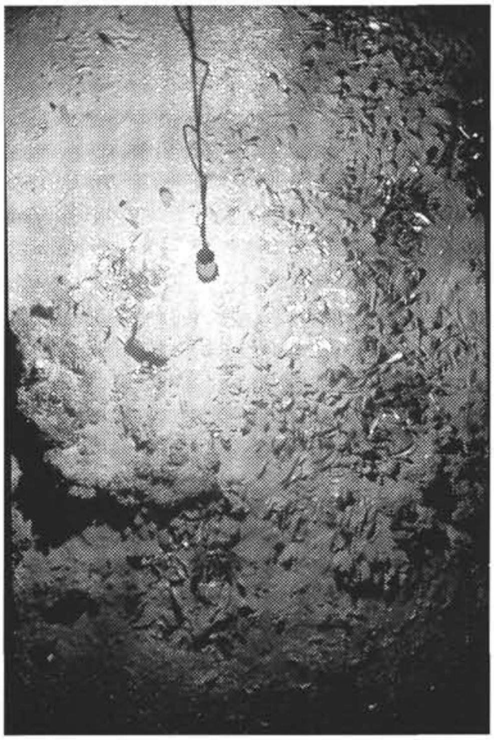

Figure 8. Seafloor photograph taken near Site 996 showing a mussel bed in the pockmark above the Blake Ridge Diapir. The photograph was taken with the Scripps Institution of Oceanography deep-tow system (Spiess and Tyce, 1973) during *Knorr* research cruise 140-1 in 1992.

Hole 996D

Hole 996D was located just outside the pockmark, ~40 m to the west of Holes 996A, 996B, and 996C. Core 164-996D-1H was retrieved with a sheared core barrel and initially was declared to have no recovery. However, some material was recovered from the drilling floor and was seen to contain a few small nodules of gas hydrate mixed with soft sediment. One nodule, estimated to be more than 100 cm^3 in size, was placed in liquid nitrogen for ~1 hr before being transferred into a gas hydrate dissociation chamber. The sample produced as much as 1530 ppm H_2S (Table 4). One ~5-cm^3 hard carbonate nodule was observed to be fizzing slightly. It was placed in a 60-mL syringe. The plunger was pushed tightly against the nodule so that the total volume was 11 mL. After 10 min, the plunger in the syringe had expanded to 14 mL, suggesting that 3 mL of gas evolved from the nodule. A small amount of gas hydrate may have been present in the nodule because the porosity of this piece of carbonate cement was very low. Some nodules of gas hydrate were examined with a binocular microscope (Figs. 15, 16). The nodules contained thin layers of clayey sediments between apparently pure layers of gas hydrate crystals. The layers of gas hydrate were 10–20 times greater in width than the clay layers.

Cores 164-996D-2X through 3X had very little recovery, and no gas hydrate was observed. Upon recovery, sediments from Core 164-996D-4H shot out of the core liner on the drilling deck. When the liner was observed on the catwalk, veins of gas hydrate were observed through the core liner in two sections. These were quickly extracted and placed into pressurized bombs for shore-based experiments. One

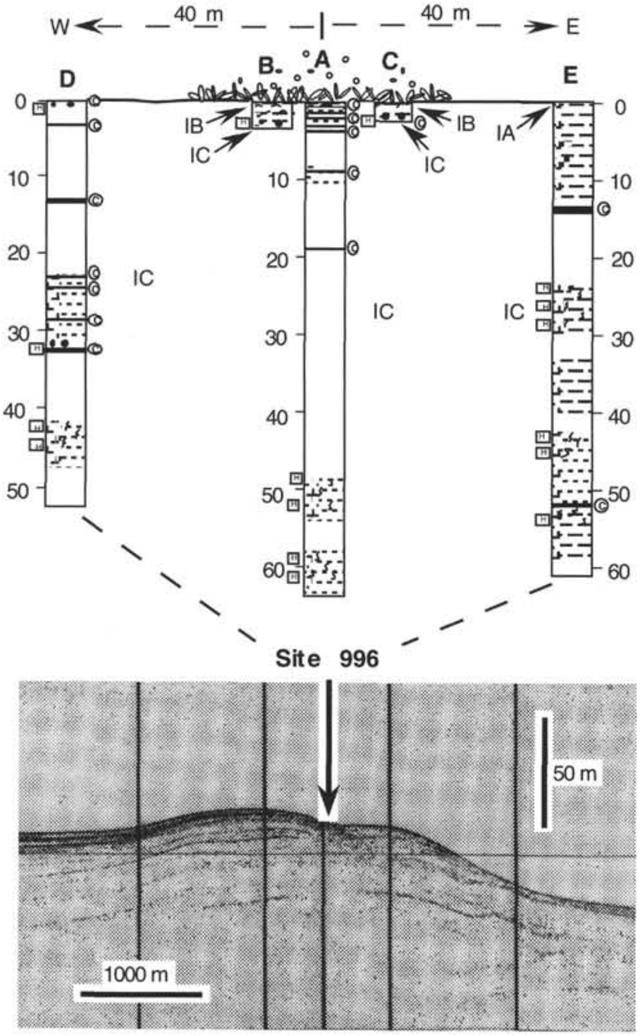

Figure 9. A 3.5-kHz echogram over the Blake Ridge Diapir showing the location of Site 996, which was drilled into a small depression on the crest of the diapir. Graphic logs show lithology for each hole (A through E). H = gas hydrate occurrence and C = carbonate nodule(s). Subunits IA, IB, and IC are indicated with arrows. Lithologic symbols are as described in the "Lithostratigraphy" section, in the "Explanatory Notes" chapter (this volume). Intervals of no recovery are blank.

Table 2. Approximate depths of carbonate concretions recovered at Site 996.

Core, section	Position (cm)	Depth (mbsf)	Remarks
164-996A-			
1H-1	0–85	0–0.85	Shell beds + nodules
1H-2	15	1.05	
1H-2	70	1.60	
1H-3	40	2.19	
1H-5	30	3.09	
1H-CC	2	3.90	
2H-CC	0–20	8.99–9.19	
4X-CC	1	19.00	
164-996B-			
1H-1	0–92	0–0.92	Shell beds + nodules
1H-2	0–105	0.92–1.97	Shell beds + nodules
164-996C-			
1H-1	0–105	0–1.05	Shell beds + nodules
2H-CC	0–20	2.40	
164-996D-			
1H-CC	0–5	0–0.05	
2X-CC	0–1	3.51	
3X-CC	0–15	13.00–13.16	
4H-1	40–50	23.00	
4H-3	50	24.52	
4H-6	120	28.44	
5X-CC	0–28	32.10–32.38	
164-996E-			
3X-CC	0–35	13.60–13.96	
6X-CC	11–22	51.62–51.73	

Note: Low recovery in some of the cores taken at Site 996 leads to uncertainties in defining the exact in situ depth of the concretions (±4 m).

piece of gas hydrate was found in the sediments on the drilling deck. However, hydrogen sulfide levels rose to more than 60 ppm on the catwalk, and sampling of the cores was postponed. Thus, many of the remaining sections were not carefully inspected for gas hydrate.

Core 164-996D-5X had poor recovery. Temperature measurements of Core 164-996D-6H were taken on the catwalk immediately after recovery, revealing several cold sections. A through-the-liner temperature measurement of −2.0°C was recorded in one part of the core (Section 164-996D-6H-7). A whole-round core sample of this anomalously cold interval was taken for preservation in a pressure vessel. The remaining sediment was squeezed for an interstitial-water sample. Sections 164-996D-6H-1 and 5 were split open immediately. They were found to contain wavy, approximately vertical veins of gas hydrate. Section 164-996D-6H-1 contained two nearly parallel veins, separated by less than 4 cm and each ~1–3 mm thick, that seemed to extend laterally across the core (Fig. 17). The veins could be traced vertically over 40 cm. Several plates of hydrate were picked out for dissociation experiments. The pieces were actively fizzing and disappeared unless preserved within 5–10 min. As they decomposed, the rate at which they disappeared seemed to increase with decreasing size, probably indicating that the rate of decomposition is a function of the surface area to volume of the sample.

Hole 996E

After termination of Hole 996D at 52.2 mbsf, the ship moved 80 m to the east. Hole 996E was located ~20 m from the pockmark on seafloor that appeared in the VIT survey. Because of potential high concentrations of H_2S (above the safety limit), initial catwalk inspections were made by a few scientists using breathing apparatuses. However, H_2S concentrations measured with the handheld meters did not exceed 2 ppm. Core 164-996E-1H recovered a 4.09-m-long core of light bluish gray clay. Measured temperatures of the sediments immediately after recovery were between 11.0° and 12.6°C, and no gas hydrate was observed. Core 164-996E-2H also had good recovery (9.05 m), and catwalk temperatures ranged between 10.0° and 15.6°C. A few millimeter- to centimeter-thick gas-expansion gaps were present in the core, but no bubbling or white material was observed in the sediments.

Core 164-996E-3X encountered hard carbonates and took ~2.5 hr to drill. Recovery was extremely low (3.8%), and only small biscuits of hard carbonate rocks were recovered in the core.

Having penetrated through the hard carbonate bed with the previous core, the APC was used to recover Core 164-996E-4H, which had moderate (71%) recovery. Before the core liner was retrieved from the core barrel, ~5 kg of sediment blew out from the top end of the core barrel. The sediment was immediately collected in a bucket and was observed to contain small, white platy fragments (3–5 mm long and 1–2 mm thick) that were fizzing. The platy white material was probably broken fragments of gas hydrate veins. Upon closer inspection, some water-ice also was observed. The water-ice is believed to have formed by the endothermic dissociation of gas hydrate. The temperature of the sediment in the bucket was as low as 1.0°C. Several parts of Core 164-996E-4H had anomalously cold (2°–4°C) temperatures, whereas other parts had temperatures between 12° and 14°C. The low-temperature portion of the core was cut off and split.

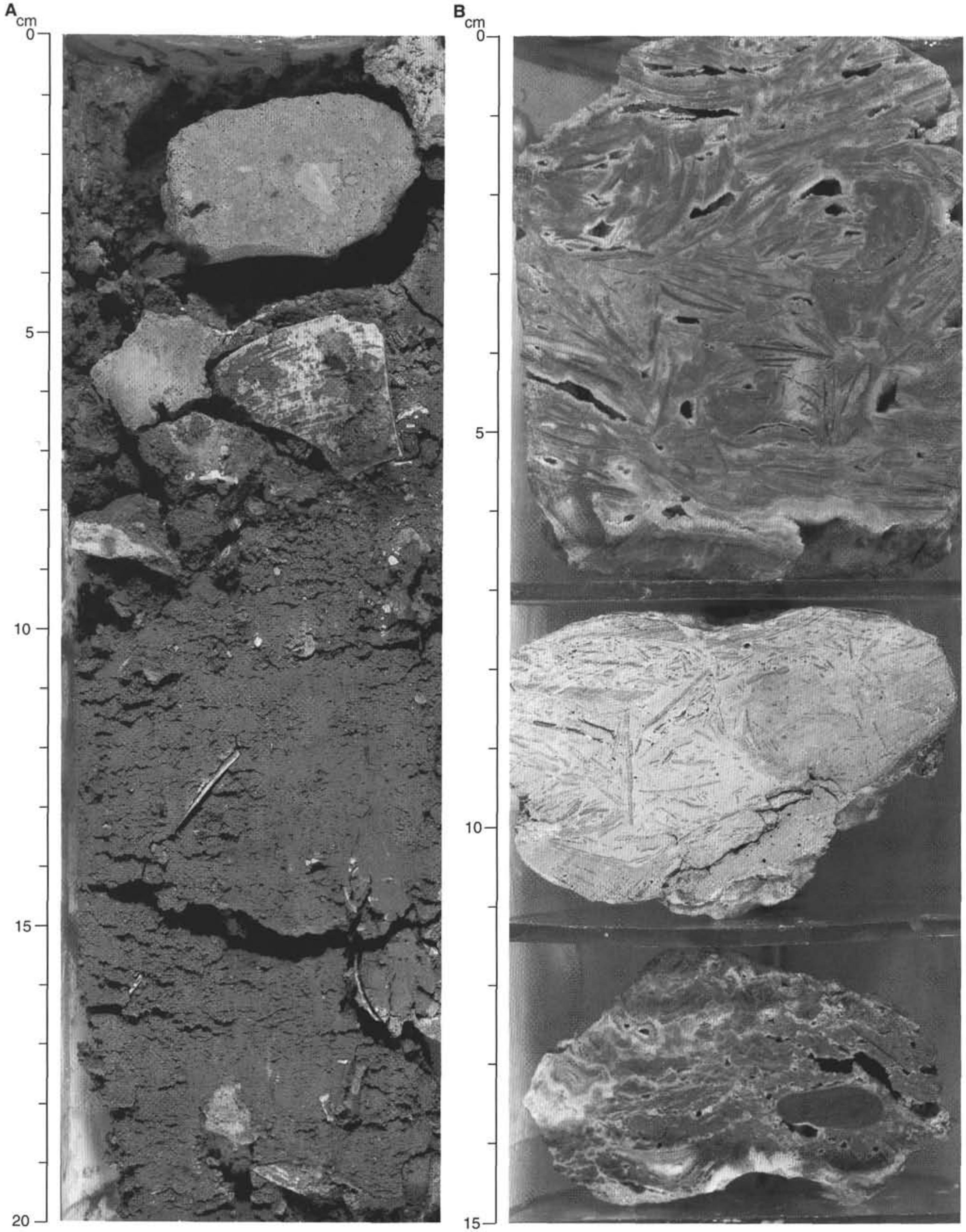

Figure 10. Carbonate nodules recovered from Site 996. **A.** Carbonate nodule with various intraclasts and surrounding sediment with bivalve shell fragments from the upper part of Hole 996A (interval 164-996A-1H-CC, 0–20 cm; 3.86–4.06 mbsf). **B.** Biocalcirudites, mainly composed of carbonate-cemented shell fragments (upper part) and calcirudites with intra- and bioclasts (lower part) from Hole 996E (interval 164-996E-3X-CC, 0–15 cm; 13.60–13.75 mbsf).

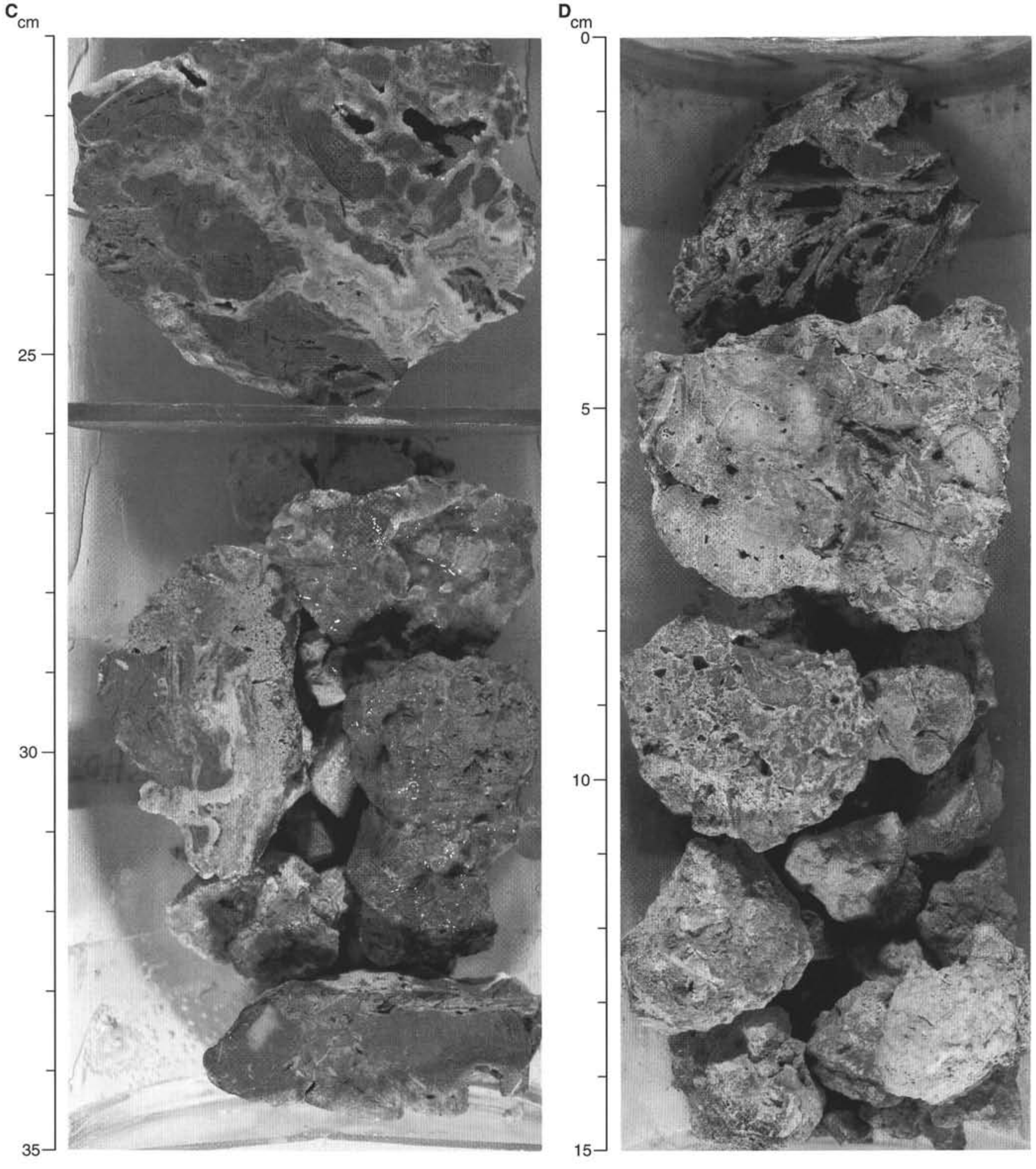

Figure 10 (continued). **C.** Calcirudites showing various generations of carbonate cement (interval 164-996E-3X-CC, 21–35 cm; 13.81–13.95 mbsf). **D.** Carbonate nodules displaying various stages of carbonate cementation (interval 164-996D-3X-CC, 0–15 cm; 13.00–13.15 mbsf).

White, platy vein hydrate and rod-shaped nodular hydrate were observed near the center of the core. The hydrate veins were oriented nearly parallel to the long dimension of the core and were broken into 1- to 3-cm-long fragments during splitting. They were bubbling and melting during inspection. Open gaps surrounded the vertical fractures where gas hydrate had apparently already decomposed.

Several rod-shaped nodules of gas hydrate, ~3 cm long and 1 cm in diameter, were observed in Section 164-996E-4H-4. The rods were oriented parallel to the long dimension of the core. They appeared to be relatively stable compared with the platy, vein hydrate. One notable feature of the rod-shaped hydrate nodules was a subtle banding, perpendicular to the long axis of the nodule, that alternated from deep

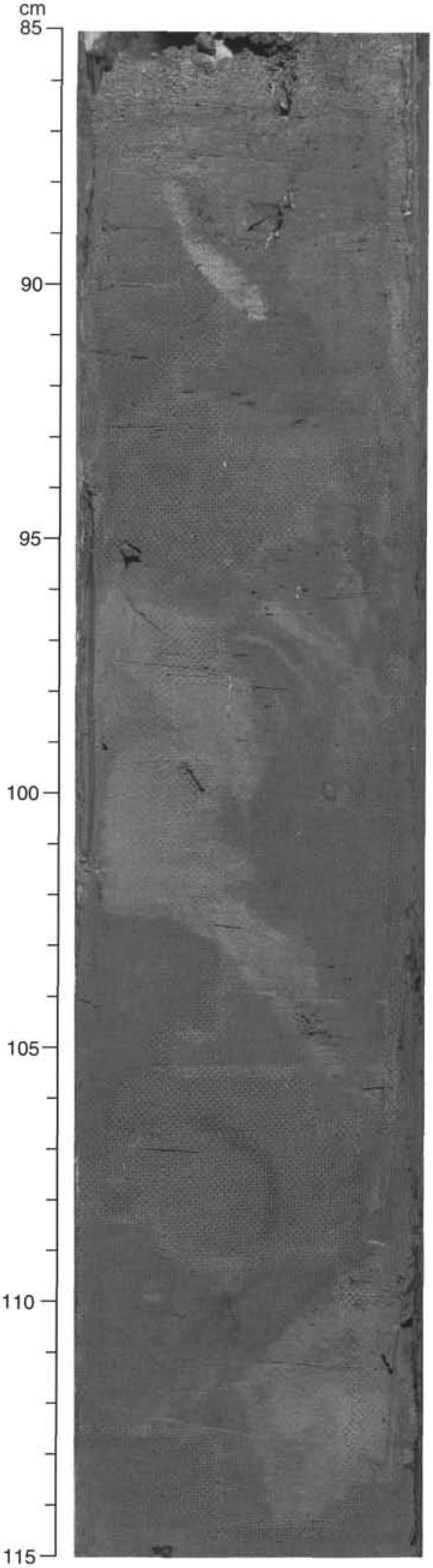

Figure 11. Deformed beds and mud clasts of variegated colors in Subunit IC (interval 164-996E-2H-1, 85–115 cm; 4.95–5.25 mbsf).

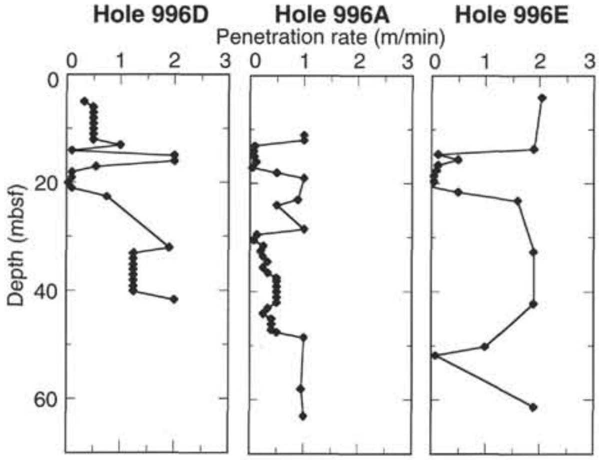

Figure 12. Sediment penetration rates during drilling at Site 996. Slow penetration corresponds to low recovery zones with hard carbonate beds.

white to slightly transparent white. Core 164-996E-4H also contained fragmented veins of hydrate in the core catcher. Because the sediments recovered in the core catcher had been moderately disturbed, the gas hydrate was fragmented into pieces several millimeters in size that bubbled and melted quickly.

Core 164-996E-5H had good recovery (79%), but no low temperatures (11.0°–12.6°C) or gas hydrate were observed. A hard layer was expected in Core 164-996E-6X based on drilling at the previous holes at Site 996, but it was not encountered. However, Section 164-996E-6X-4 was very cold (2°C) and was immediately split. Three vertically elongated nodular hydrates were seen in Section 164-996E-6X-4. They ranged in length from 4 to 12 cm and were ~2 cm across at the top, tapering to less than 1 cm at the base. The tapering was obvious in the longest nodule but not observed in the shortest (~4 cm) nodule. The surfaces of these hydrate nodules appeared transparent and shiny but were not observed to bubble. The surface of the nodules may have been coated by water-ice that was induced by dissociation of hydrate. The shape of these hydrate nodules suggested that they might have developed in sediment burrows. Numerous veins of gas hydrate also were observed and collected from Section 164-996E-6X-1. Two veins in the upper 50 cm of Section 164-996E-6X-1 displayed a cross-cutting relationship. Despite the abundant gas hydrate that was found in Core 164-996E-6X, no gas hydrate or anomalously cold intervals were found in the final APC core (164-996E-7H) recovered from Hole 996E.

Summary of Gas Hydrate Observations at Site 996

Three different types of gas hydrate occurrences were noted at Site 996:

1. Equidimensional nodules of gas hydrate were recovered from the upper few meters of sediment within the center of the pockmark under the mussel beds (Cores 164-996B-1H and 2H). These gas hydrate nodules occurred in cores that contained hazardous levels of H_2S; however, the gas hydrate itself is not believed to contain much (if any) H_2S.
2. Wavy, vertical veins of hydrate were relatively common. They were generally ~1–3 mm thick and as wide as the core, and individual veins were traceable for up to 40 cm along the surface of the cores. We infer that numerous veins similar to these are closely spaced in the sediments because two parallel veins were observed in an individual core and because veins were found in most of the cores below 30 mbsf.

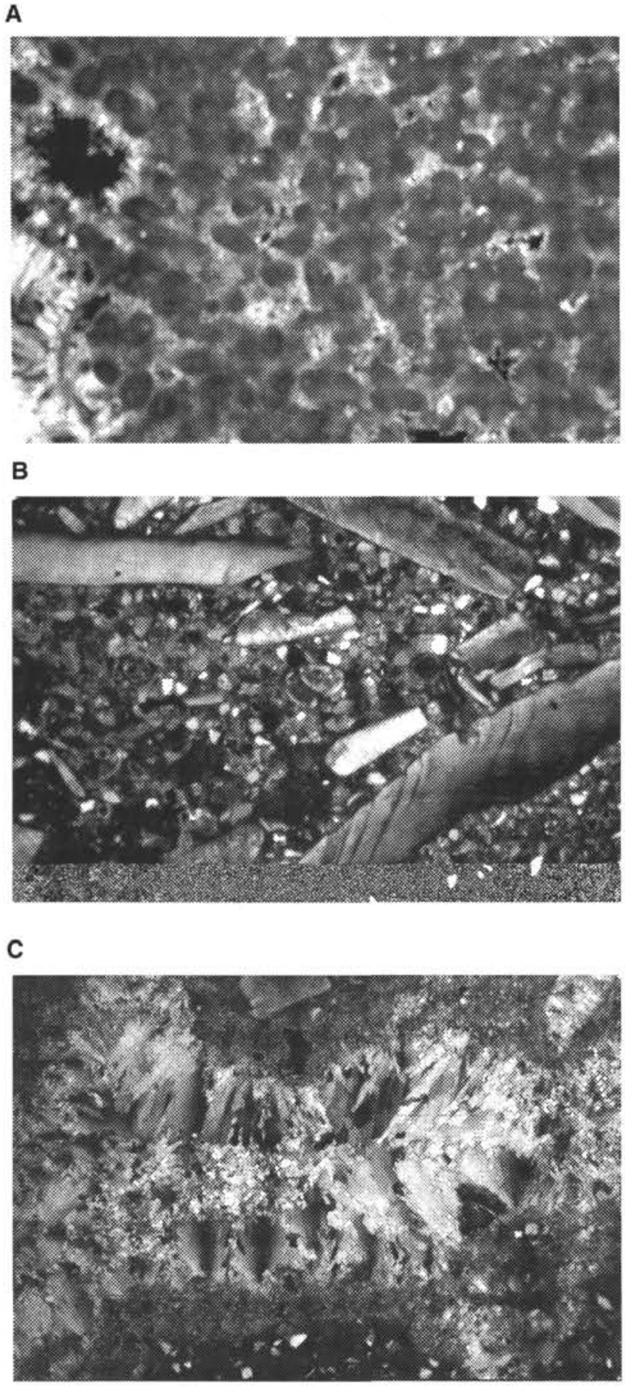

Figure 13. Photomicrographs of (**A**) peloidal micritic cement (Sample 164-996D-5H-CC, 19 cm), (**B**) biocalcarenite texture of an intraclast (Sample 164-996E-6X-CC, 17 cm), and (**C**) pore-filling cements, including radial aragonite, calcite, and equant sparite (Sample 164-996E-6X-CC, 17 cm). Photomicrographs taken with a 2.5× objective lens.

3. Vertically elongated nodules of gas hydrate, with or without a tapered lower end, were observed at ~50 mbsf at Hole 996E.

Gas Hydrate Compositions

Selected gas hydrate samples recovered at Site 996 were dissociated in a chamber, and evolved gas and meltwater were analyzed, according to the general scheme of shipboard organic and inorganic geochemistry. The results (Table 4) indicate that the gases are composed of 99.30%–99.92% CH_4, with minor amounts of CO_2 (<0.56%). Ethane concentrations ranged from 719 to 1010 ppmv. Sediment associated with gas hydrate is a possible source of the H_2S and C_3 through C_6 hydrocarbon gases. The ratio of gas to water and gas compositions indicate that these nodules consisted of structure I gas hydrate.

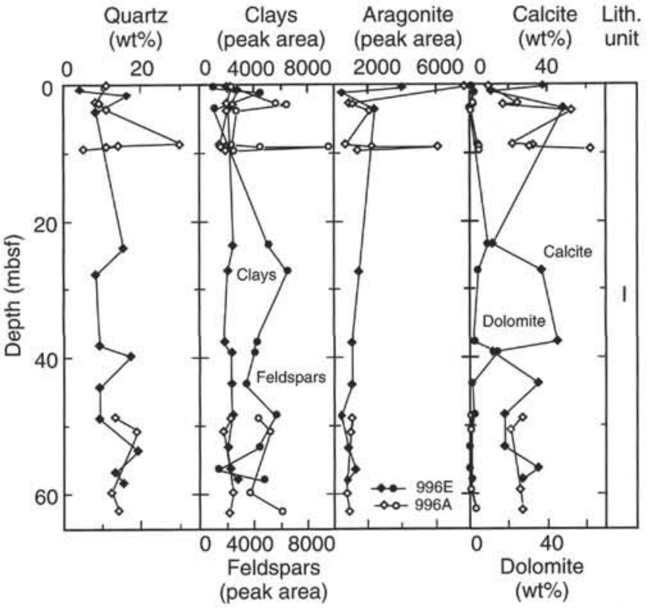

Figure 14. Downhole variations of mineral components at Site 996, based on XRD analysis. Quartz, calcite, and dolomite contents are expressed in weight percentage (see "Explanatory Notes" chapter, this volume). The relative abundances of clays, feldspars, and aragonite are given as integrated peak intensities.

Temperature Measurements

Because of generally low core recovery and H_2S hazards, systematic core temperature measurements were not conducted at Site 996. However, as in case of the previous sites, anomalously low temperatures (i.e., −2°C in Section 164-996D-6H-1) were detected in some cores in which gas hydrate was observed. Baseline temperatures of cores measured on the catwalk immediately after recovery at this site were ~12°–14°C. The distribution of measured temperatures is shown in Figure 18.

Gas-Collection Chambers

The volumes of gas that evolved from core sections while they warmed to room temperature were measured by placing whole-core sections into gas-collection chambers (see "Gas Hydrate Sampling" section, "Explanatory Notes" chapter, this volume). Table 5 gives the total volume of gas from individual whole-core sections and the estimated volume of gas that evolved per liter of interstitial pore water, calculated by assuming 60% porosity. Values are minimum estimates of the amounts of gas that were contained within the sediments in situ because the cores were actively degassing before they were placed in the gas-collection chambers.

The volumes of gas evolved from whole-core sections from Site 996 exceeded those measured for cores recovered from similar depths at previous sites (e.g., 994 and 995). However, the amounts of gas measured with the gas-collection tubes for cores recovered from the upper 63 mbsf are small in comparison with the amounts of methane that are required to saturate the waters under in situ conditions (Fig. 19). Note that the amounts of gas that are evolved from the cores are not closely related to the core temperatures at the time they are inserted into the gas-collection chambers.

Table 3. Main diffraction peak areas, d-values, and weight percentage proportions for minerals identified in samples from Site 996.

Core, section, interval (cm)	Depth (mbsf)	Quartz (101) peak area	Clay 4.4–4.6 Å peak area	Calcite (104) d-value (Å)	Calcite (104) peak area	Dolomite (104) d-value (Å)	Dolomite (104) peak area	Feldspars 3.26–3.18 Å peak area	Aragonite (111) peak area	Pyrite (311) peak area	Siderite (104) peak area	Quartz* (wt%)	Calcite* (wt%)	Dolomite* (wt%)
164-996A-														
1H-1, 34–36	0.34	15,269	2,309	3.033	6,487	2.887	1,395	2,402	7,729	398		11	10	1
1H-5, 3–4	2.82	10,735	2,057	3.034	12,555	2.891	2,301	5,650	895	616		8	25	2
1H-5, 16–18	2.95	12,463	2,486	3.035	9,785	2.89	2,380	6,449	1,137	1,304		9	17	2
1H-CC, 0–1	3.86	14,701	2,058	3.035	20,771	2.906	748	2,727	2,130	544		11	53	1
2H-1, 27–28	8.77	40,003	1,529	3.032	11,636	2.902	3,860	20,356	714	483		30	22	4
2H-CC, 9–10	9.08	14,877	1,934	3.034	15,118	2.909	3,491	4,518	2,251	515		11	33	4
2H-CC, 18–19	9.17	19,603	1,632	3.032	14,508	2.908	5,093	9,520	6,144	774		14	31	5
3X-1, 14–15	9.64	7,323	1,985	3.035	22,876	2.905	5,187	2,535	1,435	769		5	62	5
8H-1, 40–41	48.90	17,463	2,276	3.034	13,434	2.897	814	4,370	1,044	883	344	13	27	1
8H-4, 50–51	50.93	25,590	1,805	3.035	11,226	2.892	795	5,262	964	825		19	21	1
9H-2, 45–46	59.88	16,185	2,468	3.035	12,924	2.891	1,173	3,708	732	1,532		12	26	1
9H-6, 45–46	62.70	19,038	2,265	3.034	13,323	2.888	2,563	6,110	953	904		14	27	3
164-996B-														
1H-3, 37–38	2.34	13,859	2,370	3.035	9,170	2.89	2,906	6,181	766	1,580		10	16	3
1H-4, 33–34	2.92	10,008	1,920	3.035	22,159	2.905	346	3,682	1,933	504		7	59	0
164-996C-														
1H-3, 21–22	2.12	17,732	2,418	3.035	11,143	2.89	1,460	6,236	1,668	722		13	21	1
164-996D-														
4H-1, 45–46	23.05	21,140	2,171	3.033	10,207	2.889	3,556	6,332	865	740		16	18	4
4H-5, 20–21	26.56	23,238	2,068	3.034	11,080	2.905	4,639	3,940	671	1,457		17	20	5
5X-CC, 11–12	32.21	646		3.037	1,108	2.902	299		12,360	566		1	1	0
6H-2, 40–41	42.87	9,488	2,221	3.034	14,142	2.901	22,670	4,913	147	422		7	29	24
6H-5, 60–61	45.81	22,308	2,242	3.034	11,531	2.893	633	3,749	896	585		16	22	0
164-996E-														
1H-1, 43–44	0.43	7,351	1,974	3.036	16,733	2.877	791	982	4,064	793		5	38	1
1H-1, 128–129	1.28	23,087	2,751	3.033	7,136	2.89	2,449	4,474	513	459		17	11	2
1H-2, 65–66	2.15	11,742	2,193	3.035	19,294	2.889	505	1,045	2,422	1,004		9	48	0
4H-1, 27–28	23.47	21,448	2,467	3.033	7,520	2.905	8,661	5,054		1,599		16	12	9
4H-4, 45–46	27.35	12,313	2,036	3.034	16,316	2.895	4,049	6,460	1,500	506		9	37	4
5H-5, 73–74	37.78	13,165	1,791	3.035	18,518	2.909	2,378	4,152	1,085	266		10	45	2
5H-7, 44–45	39.41	24,207	2,288	3.035	7,651	2.902	13,339	4,020		861		18	12	14
6X-2, 44–45	43.95	13,972	2,301	3.035	15,966	2.895	963	3,412	1,119	462		10	35	1
6X-5, 44–45	48.45	12,960	2,444	3.034	10,255	2.894	1,953	5,594	483	1,005		10	18	2
7H-2, 63–64	53.29	26,604	2,042	3.035	10,166			4,314	851	1,304	402	20	18	0
7H-5, 79–80	56.47	18,415	2,252	3.034	15,929	2.897	317	1,391	1,342	621		14	35	0
7H-7, 9–10	58.02	21,190	2,743	3.035	13,258	2.892	1,278	4,669	834	533		16	27	1

Notes: * = percentages (wt%) for quartz, calcite, and dolomite are calculated using the calibration curves described in the "Lithostratigraphy" section of the "Explanatory Notes" chapter (this volume).

BIOSTRATIGRAPHY

Nannofossil biostratigraphy was studied on samples from Holes 996A, 996D, and 996E. All cores recovered from these holes are Quaternary in age (Fig. 20). Nannofossils are generally abundant, and preservation is mostly good except in a few samples in which advanced overgrowth hindered species identification. Reworked Cretaceous and Paleogene species are minor, but ascidian spicules are fairly common in most of the samples that were examined.

Hole 996A

Nine cores were taken from this hole, but core recovery was very poor in four cores (Fig. 20). Samples 164-996A-1H, 0–1 cm, and 1H-CC contain *Emiliania huxleyi* and are assigned to the uppermost Quaternary Zone CN15. However, *E. huxleyi* does not dominate the nannoflora, even in the mudline sample, indicating an age older than 0.085 Ma. Thus, Holocene sediment was not recovered at this hole. Samples 164-996A-2H-CC and 3X-CC yielded well-preserved nannoflora of Subzone CN14b. Small placoliths, such as small *Gephyrocapsa* and *Reticulofenestra minuta,* are particularly abundant, and rare occurrences of *Helicosphaera inversa* and *Umbilicosphaera hulburtiana* are notable.

Core 164-996A-4X recovered almost no sediment except for small pieces of cemented carbonate rubble in the core catcher. Although nannofossils frequently are present in these lithified carbonate samples, detailed taxonomic identification was difficult. However, a few taxa that belong to the genera *Coccolithus* and *Reticulofenestra* were observed.

Recovery was good in Cores 164-996A-8H and 9H. Samples 164-996A-8H-1, 38–40 cm, through 9H-CC contain few to common *Reticulofenestra asanoi* and abundant to common *Gephyrocapsa oceanica* (s. str.), indicating the lower part of Subzone CN14a (0.88–1.02 Ma) for the oldest sediment recovered at Hole 996A.

Hole 996D

Nannofossils were examined only for Cores 164-996D-4H and 6H, both of which had good core recovery. The three samples taken from Core 4H (164-996D-4H-1, 0–1 cm; 4H–3, 75–76 cm; and 4H-CC) contain abundant *Pseudoemiliania lacunosa* and *G. oceanica* (s. str.), indicating Subzone CN14a. Because no *R. asanoi* was found in these samples, the entire core (164-996D-4H) belongs to the middle to upper portion of this subzone (0.46–0.88 Ma).

Samples 164-996D-6H-1, 0–1 cm, through 6H-CC also belong to Subzone CN14a. Because these samples contain few to common *R. asanoi*, Core 164-996D-6H is assignable to the lower part of Subzone CN14a (0.88–1.02 Ma). The bottom age of Hole 996D, therefore, is same as at Hole 996A.

Hole 996E

Recovery was good throughout this hole, except in Core 164-996E-3X. Nannofossils are abundant throughout, and preservation

Table 4. Composition and gas volumes measured from samples of gas hydrate that were dissociated within a sealed dissociation chamber or gas bags.

Core, section	Total gas volume (cm^3)	Total water volume (cm^3)	Gas/water ratio (mL/L)	C_1 (%)	CO_2 (%)	H_2S (ppmv)	C_2 (ppmv)	C_3 (ppmv)	i-C_4 (ppmv)	n-C_4 (ppmv)	i-C_5 (ppmv)	n-C_5 (ppmv)	i-C_6 (ppmv)	n-C_6 (ppmv)	C_1/C_2	Cl^- (mM)
164-996A-																
1H-1	NA	NA	NA	99.31	0.43	1530	1010	12.0	1.2	0.7	1.2	0.4	NA	NA	984	NA
8H-4	NA	NA	NA	99.92	0.00	NA	772	0.5	NA	NA	NA	NA	NA	NA	1295	NA
9H-CC	NA	NA	NA	99.92	0.00	NA	754	6.8	1.7	0.7	1.7	NA	0.1	NA	1325	NA
164-996B-																
1H-1	346.7	6.5	53	99.30	0.56	390	969	11.9	2.5	0.6	2.7	0.5	0.5	0.3	1025	169
1H-1	182.5	9.1	20	99.41	0.51	90	753	8.9	1.7	0.4	2.0	0.4	0.2	0.4	1320	248
164-996C-																
1H-1	195.4	3.3	65	99.46	0.43	348	719	7.3	1.6	0.5	1.1	0.4	NA	NA	1383	294
1H-1	369.2	4.8	78	NA	NA	NA	NA	NA	NA	NA	NA	NA	NA	NA	NA	245
1H-2, 0–1 cm	61.2	1.9	32	99.83	0.00	NA	857	15.8	4.3	0.9	3.1	0.8	0.4	0.4	1166	352
164-996D-																
5X-1	235.6	3.5	67	99.66	0.27	NA	747	18.3	3.2	0.8	3.9	0.7	0.3	0.3	1334	317
6H-1	NA	NA	NA	99.60	0.33	40	744	10.9	2.4	0.6	3.2	0.6	0.2	0.3	1338	NA
164-996E-																
6H-5	NA	NA	NA	99.60	0.33	NA	744	10.9	2.4	0.6	3.2	0.6	0.2	NA	1338	NA
7H-CC	907.8	6.4	143	99.70	0.23	NA	719	6.9	1.6	0.4	1.8	0.5	0.2	NA	1387	21

Notes: Gas compositions are normalized to 100%. Oxygen and nitrogen were detected but eliminated from this calculation because they are considered contaminants. NA = not analyzed.

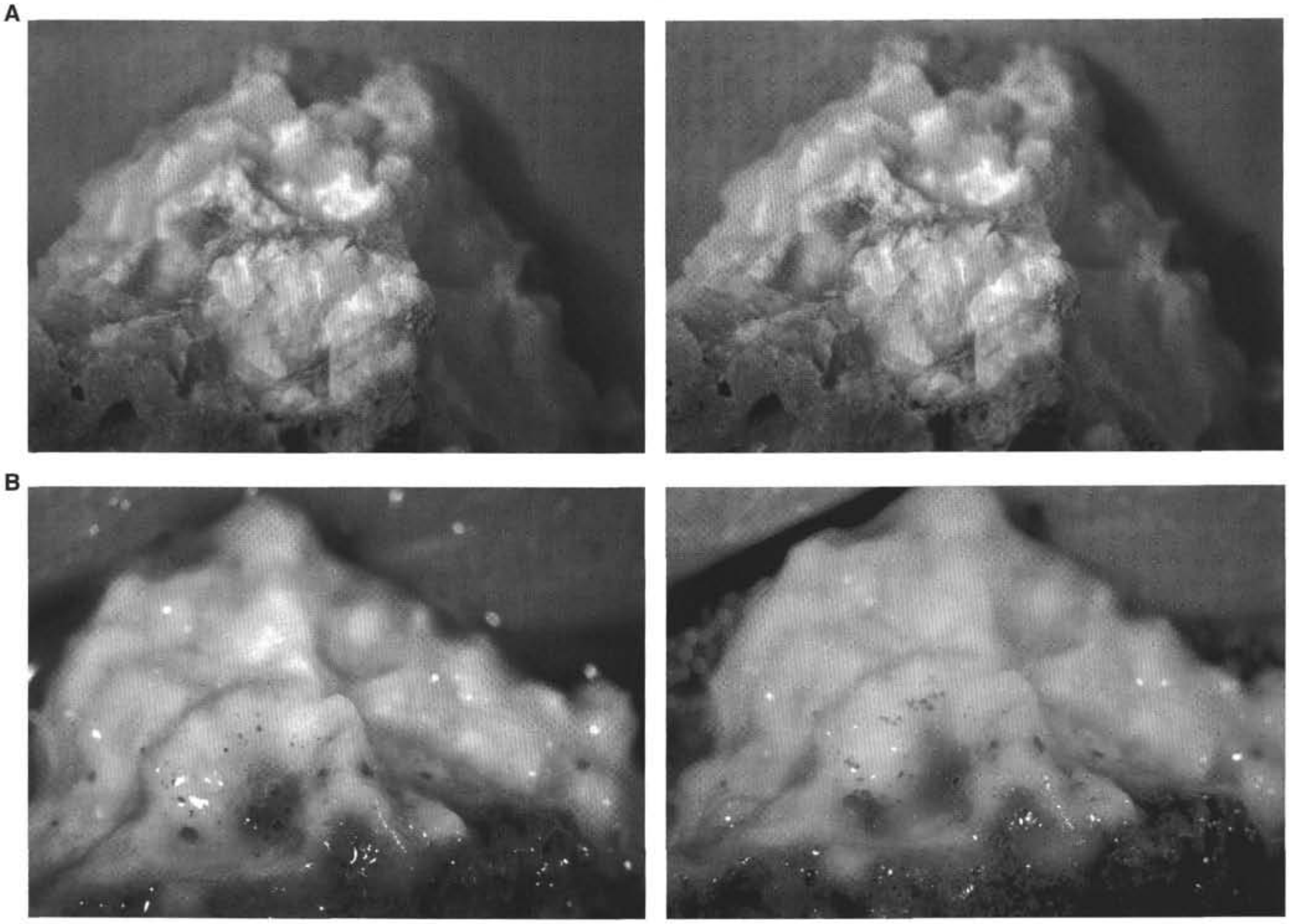

Figure 15. Photomicrographs showing the crystal habit of gas hydrate recovered from Section 164-996D-1H-CC. Stereo-photomicrographs taken (**A**) soon after recovery and (**B**) 11 min after the sample was left at room temperature (~20°C). Photomicrographs taken with a 2.5× objective lens.

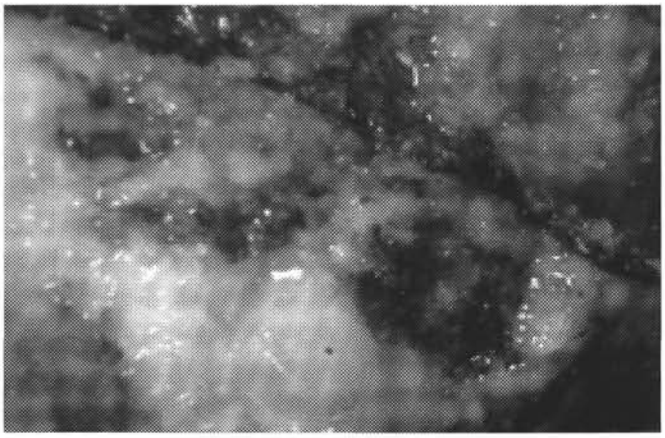

Figure 16. Photomicrograph of the surface of a gas hydrate nodule from Section 164-996D-1H-CC. White material is mostly gas hydrate, as evidenced by bubbling, but some water-ice also may be present. Shiny transparent surfaces are covered with water, which is in part generated by the decomposing hydrate. Dark materials are clay layers and inclusions. Field of view = ~3 mm.

was good except in two samples (out of 35 samples examined) in which moderately advanced overgrowth and weak dissolution were observed.

E. huxleyi dominates the nannoflora in Samples 164-996E-1H-1, 9–10 cm, and 1H-2, 39–41 cm—a clear indication of the Holocene or uppermost Pleistocene (<0.085 Ma). The first occurrence (FO) of *E. huxleyi* is between Samples 164-996E-2H-4, 39–41 cm, and 2H-5, 39–41 cm; therefore, the lower part of Core 164-996E-2H belongs to Subzone CN14b (0.27–0.46 Ma).

Samples 164-996E-4H-1, 39–41 cm, through 6X-2, 39–41 cm, contain nannoflora of Subzone CN14a, and the last occurrence (LO) of *R. asanoi* (0.88 Ma) was observed in Sample 164-996E-6X-1, 39–41 cm. Although preservation is generally good in this interval, nannofossils are moderately overgrown, particularly in Sample 164-996E-4H-1, 39–41 cm (23.60 mbsf). The occurrence of overgrown coccoliths is not surprising because there are indulated carbonate layers nearby (e.g., Core 164-996A-4H). Small *Gephyrocapsa* dominates the flora, and *G. oceanica* is absent in Samples 164-996E-6X-3, 39–41 cm, through 6X-CC, which is a clear indication of the "small *Gephyrocapsa* Zone" corresponding to the latest part of Subzone CN13b.

In the six samples examined from Core 164-996E-7H, abundant to common *G. oceanica* (s. str.) and frequent *R. asanoi* were observed. This flora is identifiable to the lower part of Subzone CN14a. There are five possible explanations for this reversed age phenomenon: (1) the sequence recovered in Cores 164-996E-5H and 6X is a slump deposit, (2) a reversed fault exists between Cores 164-996E-6X and 7H, (3) an early Pleistocene form of genus *Gephyrocapsa* that occurs in the lower upper portion of Subzone 13b was misidentified as *G. oceanica* (s. str.), (4) repeated coring took place by accident, or (5) younger material fell down the hole (a crushed mussel with fresh tissue, which apparently fell down the hole, was recovered from Core 164-996A-4X).

Sedimentation Rate

Because of the poor recovery, the sedimentation rate is difficult to estimate for Holes 996A and 996D. Assuming no structural disturbance for the upper six cores, the sedimentation rate for the late Pleistocene is 48 m/m.y. at Hole 996E (Fig. 21), which is similar to the Quaternary rate obtained at the Blake Ridge sites (994 and 995).

PALEOMAGNETISM

Magnetostratigraphy

Paleomagnetic measurements at Holes 996A, 996D, and 996E were carried out with the pass-through cryogenic magnetometer, following the procedures outlined in the "Paleomagnetism" section, "Explanatory Notes" chapter (this volume). We measured the NRM on the archive half of core sections and demagnetized them under an AF of 10 mT to determine the direction of the stable component of remanence. To supplement magnetostratigraphic results from the routine demagnetization, eight discrete samples from Hole 996A, three from Hole 996D, and eight from Hole 996E were AF demagnetized in 5-mT steps up to 55 mT.

The NRM intensity of the three holes is generally between 10 and 0.1 mA/m, with scattered measurements of high intensity >100 mA/m (Fig. 22). The higher NRM measurements occur at the top of each core, suggesting contamination from drill pipe rust. The NRM declinations are very scattered, and the inclination is generally downward (positive), frequently near +90°.

After demagnetization at 10 mT, intensity is generally 0.1 mA/m (Fig. 22). The inclination after 10-mT demagnetization shifts toward lower inclinations and is more scattered than that of NRM. The decrease in intensity and inclination suggests that demagnetization has removed the core-barrel overprint.

Progressive AF demagnetization of the discrete samples shows that the steeply downward-inclined drilling-induced components can be removed from most samples, leaving a stable component of remanence at 5 mT (Fig. 23). After the removal of the overprint, typical progressive demagnetization up to 55 mT follows a linear demagnetization path that converges on the origin of the Zijderveld plot (Fig. 23). This indicates a single, stable component that is interpreted as the primary remanence, from which magnetic polarity can be determined.

Polarity determined from the analysis of the discrete samples does not correlate well with the inclination data obtained from the 10-mT demagnetization of continuous core sections in the cryogenic magnetometer (Fig. 24). Apparently, the cryogenic magnetometer record does not reveal the primary magnetization. The difference between the discrete sample and pass-through data may result from limitations of the cryogenic magnetometer in measuring very weak magnetization (see "Paleomagnetism" section, "Explanatory Notes" chapter, this volume).

Approximate positions for polarity chron boundaries were estimated on the basis of the polarity data of the discrete samples with the constraint of the nannofossil datums (see "Biostratigraphy" section, this chapter; Fig. 24). In Hole 996E, the C1n/C1r.1r chron boundary (Matuyama/Brunhes boundary) is tentatively placed at ~33 mbsf, and the C1r.1r/C1r.1n boundary (the top of the Jaramillo normal chron) at ~40 mbsf. In Hole 996A, a reversed polarity at 49.97–49.99 mbsf is correlated to the polarity chron C1r.1r within the nannofossil zone CN14a, and so the Matuyama/Brunhes boundary is between 10 and 50 mbsf in Hole 996A and below 26 mbsf in Hole 996D.

Magnetic Susceptibility

Measurement of magnetic susceptibility of whole-core sections at Site 996 using the MST was interrupted by discontinuous core recovery, gas voids, and the removal of whole-round cores. Only in Hole

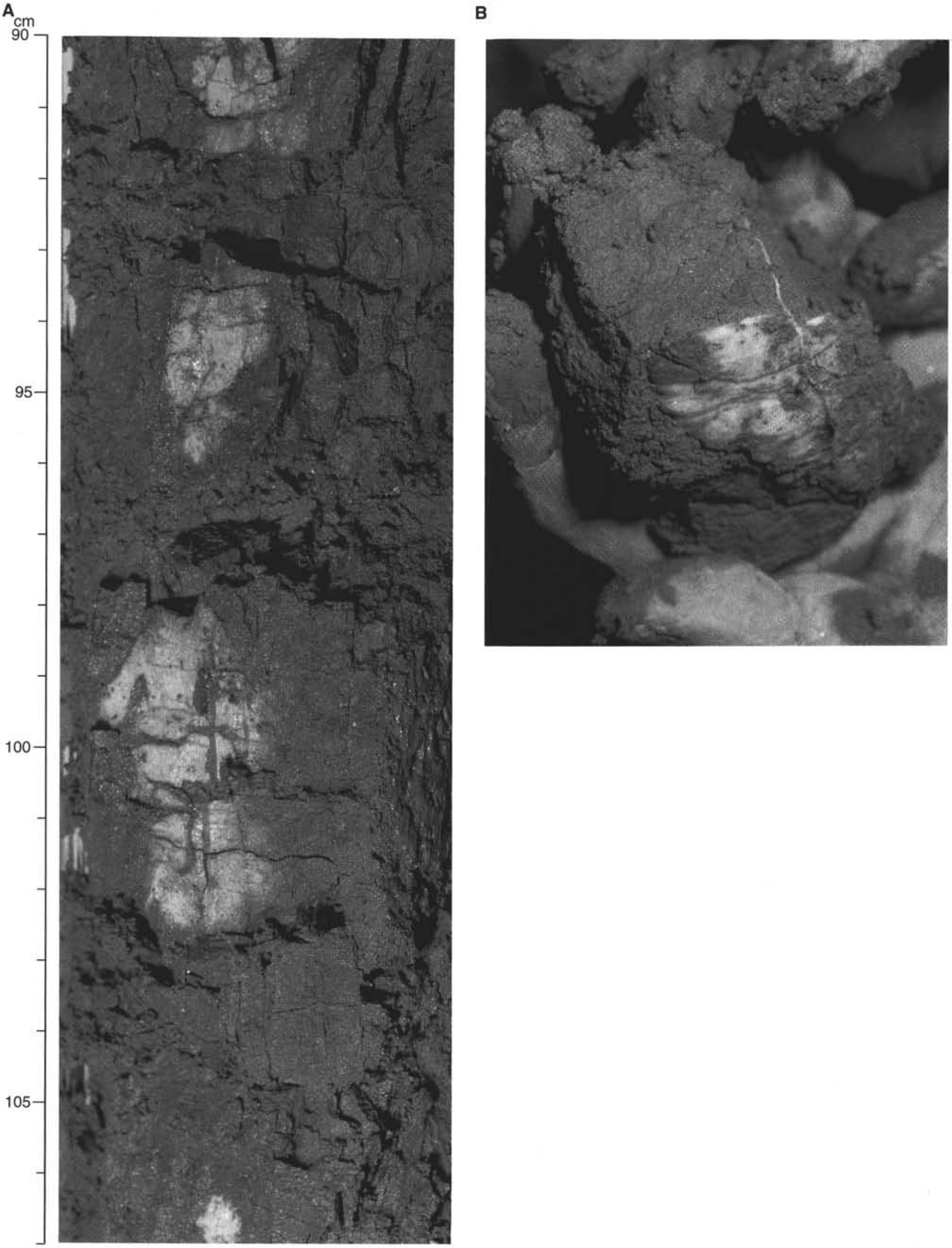

Figure 17. Photographs of vein-type gas hydrate that fills vertically running fractures. **A.** Interval 164-996D-6H-1, 90–107 cm. **B.** Hand specimen from the same interval. Note the cross-cutting gas hydrate veins in (B).

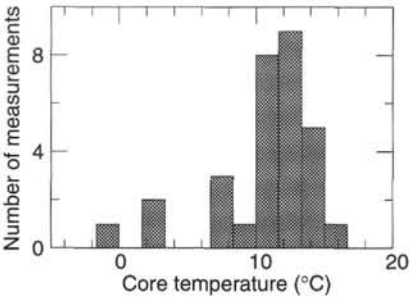

Figure 18. Distribution of core temperatures measured at the catwalk at Site 996. Anomalously low temperatures indicate either the presence of gas hydrate or water-ice that formed because of endothermic dissociation of gas hydrate or the expansion of gas.

Table 5. Volumes of gas collected from 1.5-m whole-core sections as they warmed to room temperature inside gas-collection chambers.

Core, section	Depth to top of section (mbsf)	Insertion temperature (°C)	Gas evolved (mL)	Gas/pore water ratio (mL/L)
164-996A-				
8H-4	53	13.0	1756	358
9H-6	62	5.0	102	20
164-996D-				
4H-4	22	13.0	142	29
6H-3	45	5.0	2046	417
164-996E-				
1H-2	5.6	12.0	0	0

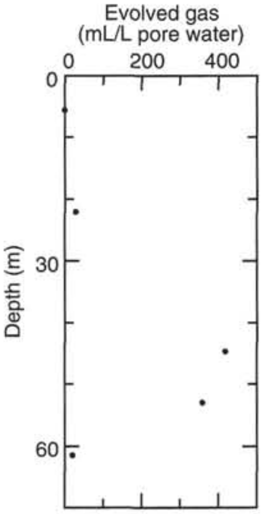

Figure 19. Plot of the volume of gas that was evolved per liter of pore water from 1.5-m whole-core sections as they warmed to room temperature. The total amount of gas was corrected by the porosity of the cores to give mL of pore water.

996E was recovery sufficiently continuous to allow the downhole trend in susceptibility to be characterized (Fig. 25); shorter intervals measured in the other holes at Site 996 are consistent with the susceptibility profile of Hole 996E.

No interval of elevated susceptibility is present in the first few meters below seafloor at Site 996, which suggests that there is no zone at this site in which magnetite authigenesis dominates iron reduction processes. A magnetite authigenesis zone was identified at all other sites during Leg 164, with the exception of Site 993, where recent removal of the Pliocene–Pleistocene section explains the absence of such a zone (see "Paleomagnetism" section, "Sites 991/992/993" chapter, this volume). Similar removal of a pre-existing magnetite authigenesis zone at Site 996 is inconsistent with evidence for continuous sedimentation, at least in Hole 996E (see "Lithostratigraphy" and "Biostratigraphy" sections, this chapter).

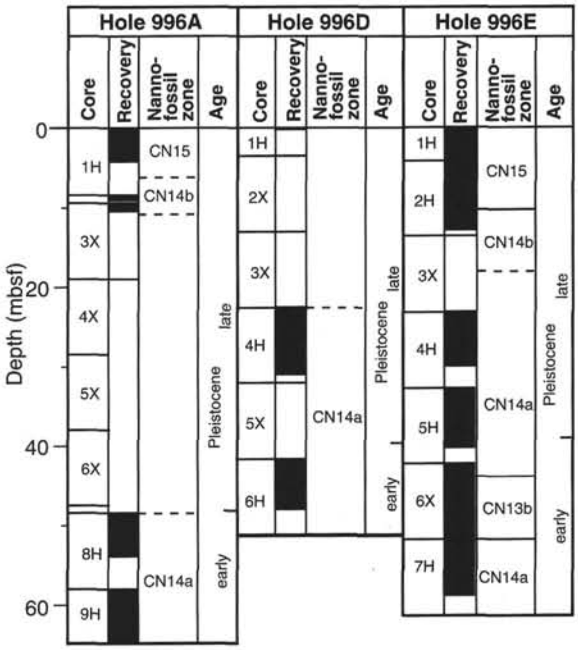

Figure 20. Biostratigraphic summaries of Holes 996A, 996D, and 996E. Dashed lines indicate stratigraphic uncertainties.

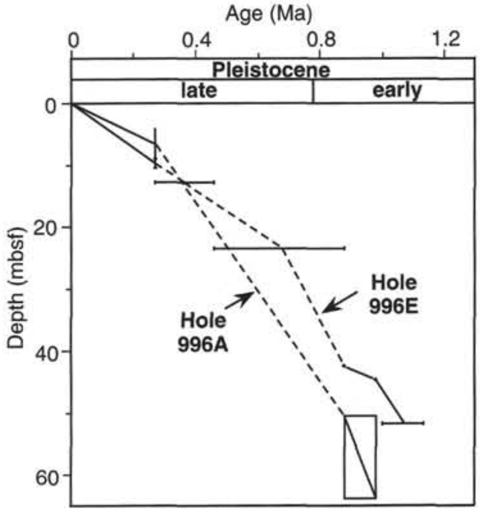

Figure 21. Age-depth relationships of biostratigraphic markers of calcareous nannofossils at Holes 996A and 996E. Age and depth uncertainties are indicated by horizontal and vertical bars, respectively; the rectangular box indicates the combined age-depth uncertainty.

Rock Magnetism

Saturation Isothermal Remanence

Within the short interval cored at Site 996, no systematic trend in SIRM could be discerned; SIRM normalized for bulk susceptibility

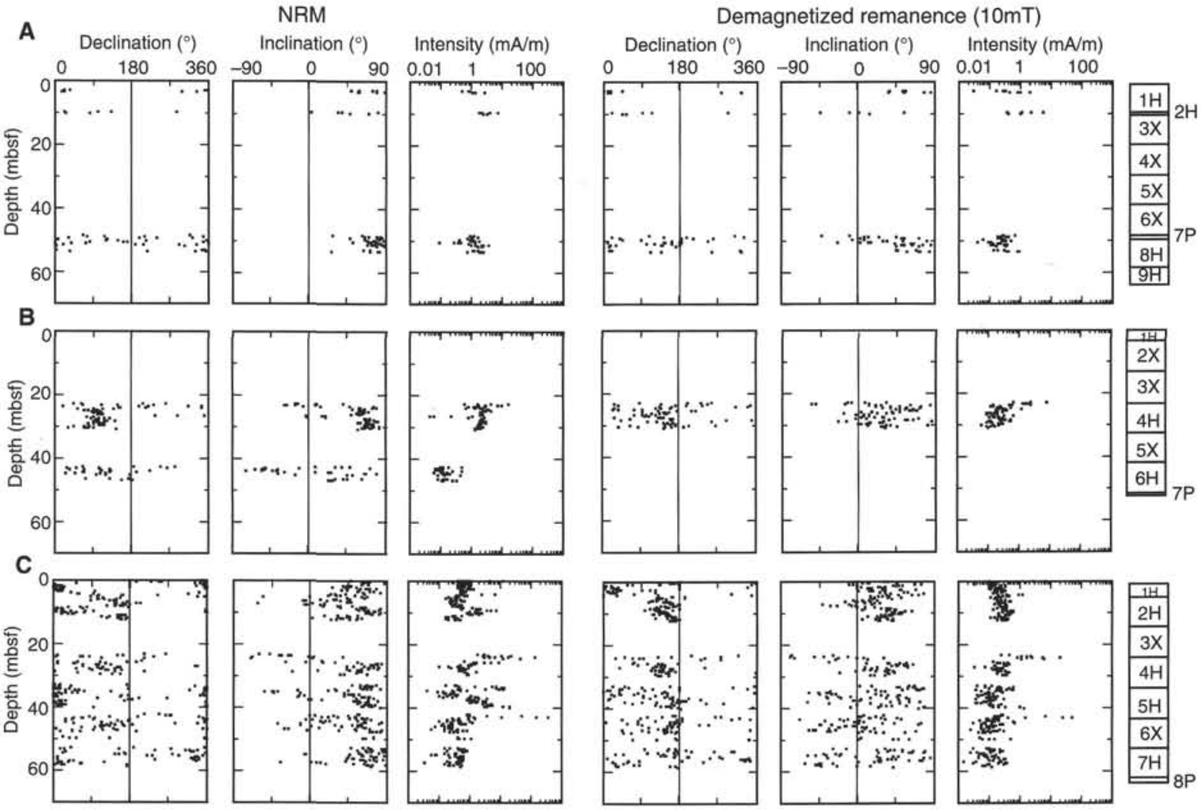

Figure 22. Declination (referred to arbitrary core coordinates), inclination, and intensity of NRM and remanence after 10-mT demagnetization at (**A**) Hole 996A, (**B**) Hole 996D, and (**C**) Hole 996E.

(SIRM/k) is scattered between 600 and 3000 A/m in both Holes 996A and 996B (Fig. 26A). The range and scatter of SIRM/k values are similar to those observed at Sites 994 and 995 in the upper part of the gas hydrate stability field, above the zone of gas hydrate recovery and low pore-water chloride concentrations. The scatter in SIRM/k at Site 996 contrasts with the systematic downhole trends in SIRM/k at Sites 991, 992, and 993, where interstitial-water chloride concentrations are anomalously high. Values of SIRM/k exceeding 10 kA/m, which characterize the magnetite authigenesis zone in the first few meters below seafloor at Sites 991, 992, 994, and 995, are absent from Site 996.

Coercivity

All three coercivity measures at Site 996—the $S_{-0.3T}$ ratio, the acquisition of pIRM, and the acquisition of pARM—indicate the absence of an initial zone dominated by magnetite authigenesis. The $S_{-0.3T}$ ratio never exceeds 0.94 in any samples measured at this site (Fig. 26B) and is only 0.89 in Sample 164-996E-1H-1, 53–55 cm, taken at only 0.53 mbsf. In the magnetite authigenesis zone at other sites during Leg 164, $S_{-0.3T}$ is always ≥0.95. Coercivity spectra defined by pARM at Site 996 are either left skewed, with a peak at 15 mT, or are very broad (Fig. 27). None show a single, well-defined peak at ~35–45 mT, which would indicate the presence of substantial proportions of pseudo-single domain (PSD) to SD magnetite, as is the case with samples in the first few meters below seafloor at Sites 991, 992, 994, and 995. Coercivity at higher field strengths, defined by pIRM spectra, indicate the presence of magnetic phases other than magnetite throughout the sequence at Site 996 (Fig. 28); the pIRM spectra are similar to those observed at Site 995, where greigite (and tentatively, pyrrhotite) were identified in XRD analyses.

Summary of Susceptibility and Rock Magnetism

Site 996 differs from all other Leg 164 sites (with the exception of the truncated top of Site 993) in lacking a zone in which bacterial authigenesis of magnetite dominates iron reduction. Instead, iron reduction at Site 996 apparently progresses to the generation of magnetic iron sulfides at <0.5 mbsf. Site 996 displays scattered SIRM/k values between ~600 and 3000 A/m, similar to the upper parts of the gas hydrate stability zone at Sites 994, 995, and 997 but extending to much shallower sub-bottom depths. Site 996 apparently shares with Sites 994, 995, and 997 the relationship between the upper part of the hydrate stability field, and the generation and preservation from further reduction to pyrite, of significant proportions of magnetic iron sulfides. However, fault-mediated transport of methane at Site 996, and the subsequent concentration of hydrate and H_2S within a few meters of the seafloor, has evidently resulted in the extensive production of greigite at shallow sub-bottom depths. Similar concentrations of magnetic sulfides were indicated by rock-magnetic methods within a near-seafloor occurrence of gas hydrate at Site 892 on the Cascadia Margin (Shipboard Scientific Party, 1994; Housen and Musgrave, 1996). Methane venting and H_2S accumulation in association with a fault that displaced the BSR are features common to both Site 996 and Site 892.

DOWNHOLE TOOLS AND SAMPLING

Pressure Core Sampler

Abundant gas hydrate was observed in sediment from APC and XCB cores at Site 996 (see "Gas Hydrate" section, this chapter). The PCS was deployed three times at Site 996 (Table 6) in an effort to col-

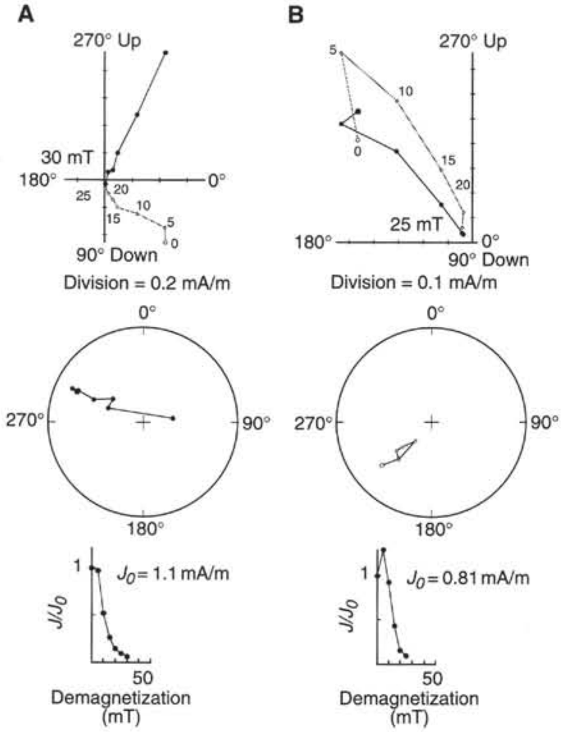

Figure 23. Representative Zijderveld, stereo, and intensity demagnetization plots for (**A**) Sample 164-996A-3X-1, 37-39 cm (9.87–9.89 mbsf), which is normally polarized, and (**B**) Sample 164-996A-8H-3, 14–16 cm (49.97–49.99 mbsf), which is reversely polarized. Demagnetization increases in 5-mT steps to 30 mT for (A) and 25 mT for (B). Zijderveld plot: solid circles = projection on the horizontal plane; open circles = projection on the vertical plane. Stereo plot: solid circles = the lower hemisphere. Declination is with respect to core coordinates.

lect sediment with gas hydrate at in situ pressure. However, because ample gas hydrate was available for sampling and analysis from the APC and XCB cores, the cores in the PCS were used to examine gas evolution during hydrate dissociation rather than for actual hydrate collection.

The general procedure for taking gas samples from the PCS was the same as that performed at Site 995 (see "Downhole Tools and Sampling" section, "Site 995" chapter, this volume). The major difference was the number of gas samples taken from Cores 164-996A-7P and 996D-7P. Twenty-five and 20 aliquots of gas were taken from Cores 164-996A-7P and 996D-7P, respectively. Each of these aliquots is a 10- to 50-mL portion of a larger "split" of gas (10–1060 mL) that was released at a certain pressure (and cumulative volume) as the PCS was slowly depressurized (Table 6; Fig. 29). The gas composition of each aliquot is presented in Table 7.

Core Description

Core 164-996A-7P (47.5 mbsf) had 102% of hydrostatic pressure after recovery (Table 6). The PCS contained 20 cm of core and evolved 5415 mL of gas. Several cubic centimeters of greenish gray sediment also passed through the PCS-M. The core within the PCS was composed of abundant broken shell fragments with a minor amount of clay matrix.

Core 164-996D-7P (51.2 mbsf) had 91% of hydrostatic pressure after recovery (Table 6). The core contained 8100 mL of gas but no sediment. However, several cubic centimeters of greenish gray sediment slurry came out of the PCS-M.

Core 164-996E-8P (61.3 mbsf) had only 29% of hydrostatic pressure at the PCS sampling station. The core contained 575 mL of gas, most of which (450 mL) contained >84% CH_4 (Table 7). No sediment core was found in the PCS although several cubic centimeters of greenish gray sediment slurry was observed to come out of the PCS-M.

The "Disappearance" of Core 164-996D-7P

Repeated tests at Sites 995 and 997 have demonstrated that PCS "cores" recovered without sediment are filled with borehole water that evolves only air and small amounts of CH_4. These tests also have shown that the total volume of gas from borehole water is <200 mL. Thus, essentially all CH_4 from a PCS core comes from sediment in the PCS.

Core 164-996D-7P released approximately 8 L of CH_4 but did not contain sediment when the PCS was opened after degassing. Only one explanation is consistent with PCS experiments and observations at other Leg 164 sites: gas hydrate must have been in the PCS. Simple calculations indicate that the amount of hydrate was ~ 48 cm^3.

Gas Evolution Experiments: Preliminary Interpretations

There are obvious variations in gas composition with respect to time, volume, and pressure for Cores 164-996A-7P and 996D-7P (Table 7; Fig. 29). The first few aliquots of gas, collected at high pressure, have low concentrations of air (N_2 and O_2) and CH_4. This is because the first samples (<60 mL cumulative volume) contain significant amounts of He that resides in the PCS-M before each run. The next few aliquots (<100–200 mL cumulative volume) contain significant amounts of air and relatively low concentrations of CH_4. Tests at Sites 995 and 997 (see "Downhole Tools and Sampling" sections, "Site 995" and "Site 997" chapters, this volume) indicate that 100–200 mL of air is routinely trapped inside the PCS (probably within the mandrels) during deployment.

Large volumes of CH_4 are released when the pressure in the PCS decreases below a value between 400 and 500 psig. The consistent release of CH_4 in this pressure range (see "Downhole Tools and Sampling" sections in other site chapters, this volume) suggests that a phase boundary is being crossed. The last aliquots of gas are relatively enriched in air. The source of this air is unknown.

There is an intriguing trend in the C_1/C_2 ratio with respect to cumulative volume that is observed for both Cores 164-996A-7P and 996D-7P (Fig. 30). At low cumulative volumes, the C_1/C_2 ratio is relatively low (excepting the first two gas splits from Core 164-996A-7P). Then there is an interval with relatively high C_1/C_2 values at intermediate cumulative volumes. The last few splits have the lowest C_1/C_2 ratios. The cause of this change is unclear with available information.

ORGANIC GEOCHEMISTRY

The shipboard organic geochemistry program at Site 996 included analyses of volatile hydrocarbons, carbon dioxide, and hydrogen sulfide as well as determinations of inorganic carbon, total nitrogen, total carbon, and total sulfur in sediment (for a description of methods, see "Organic Geochemistry" section, "Explanatory Notes" chapter, this volume).

Volatile Hydrocarbons

Headspace Gases

Headspace methane (C_1) concentrations in sediment from Hole 996A range from 6,300 µL/kg at 0.9 mbsf to 44,800 µL/kg at 59.4 mbsf. Headspace ethane (C_2) concentrations are between 2 and 34

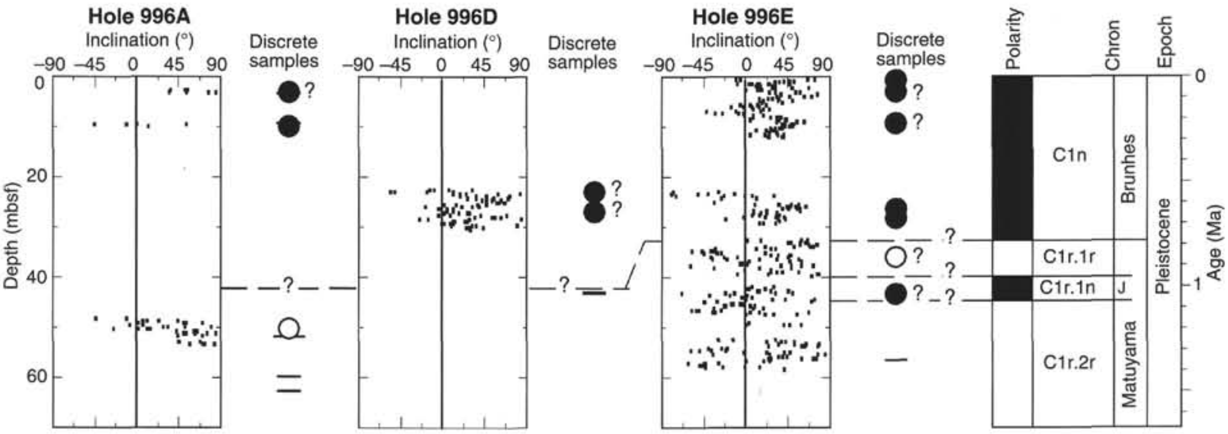

Figure 24. Inclination after 10-mT demagnetization with pass-through magnetometer and polarity data determined from Zijderveld diagram analysis of discrete samples from Site 996, correlated to the revised geomagnetic polarity time scale of Cande and Kent (1995). Solid circles and zones = normal polarity, open circles and zones = reversed polarity, question marks (?) = less certain polarity, and bars = unsuccessful analyses. J = Jaramillo.

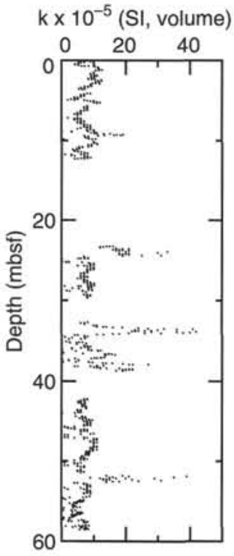

Figure 25. Susceptibility determined on the MST of cores from Hole 996E.

μL/kg, and headspace propane (C_3) concentrations are between 0 and 18 μL/kg. Higher molecular weight hydrocarbons up to heptane (C_7) also were detected in trace amounts (Table 8).

Hydrocarbon concentrations in sediment from Holes 996C and 996D are about the same as those in sediment from Hole 996A. Because of the small number of samples, depth trends could not be established with confidence.

In contrast, C_1 concentrations in sediment from Hole 996E increase within a short distance from 93 μL/kg in Core 164-996E-1H (1.5 mbsf) to 55,400 μL/kg in Core 2H (5.6 mbsf). Concentrations of C_1 are ~30,000 μL/kg (Table 8) at depths of 42.2 and 51.8 mbsf.

Free Gas

Most gas samples recovered from core liners contain more than 900,000 ppm C_1. Air contamination accounted for the balance of total gas. The C_2 concentrations range from 628 to 937 ppm, and the C_1/C_2 ratio varies from 1060 to 1610. Higher molecular weight compounds occur in all samples: propane (C_3) reaches 23 ppm; isobutane (i-C_4) and isopentane (i-C_5) range from 1 to 10 ppm. Carbon dioxide (CO_2) concentrations vary between 0.6% and 2.1%. A maximum value of 5.3% hydrogen sulfide (H_2S) was measured in a Hole 996A sample from a depth of 10.0 mbsf (Fig. 31; Table 9).

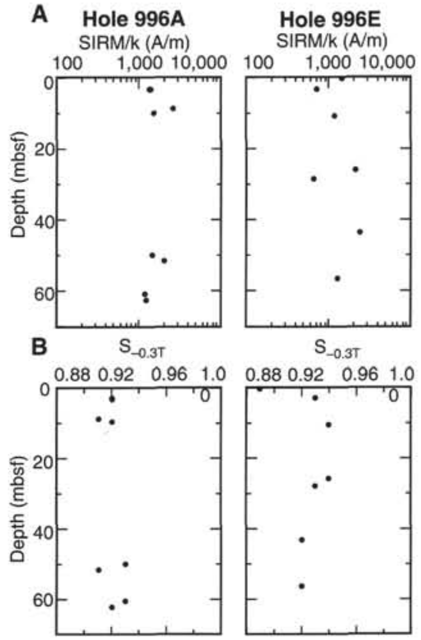

Figure 26. (**A**) SIRM/k and (**B**) $S_{-0.3T}$ vs. sub-bottom depth.

Gas-Collection Chamber Gases

GCC gases are diluted as much as 95% with air. The C_1 concentrations from the GCC are 1 to 2 orders of magnitude higher than corresponding C_1 concentrations in headspace gas (Table 10). Direct comparison of results from the GCC and headspace sampling methods is difficult because volumes of sediment and headspace gas are much different in the two techniques. Ratios of C_1/C_2 are slightly higher in GCC gas relative to free gas.

Content of Organic Carbon, Total Nitrogen, and Total Sulfur

The TOC and organic nitrogen content of most sediment is <0.5% (Fig. 32; Table 11) and <0.1%, respectively. Meaningful C/N ratios

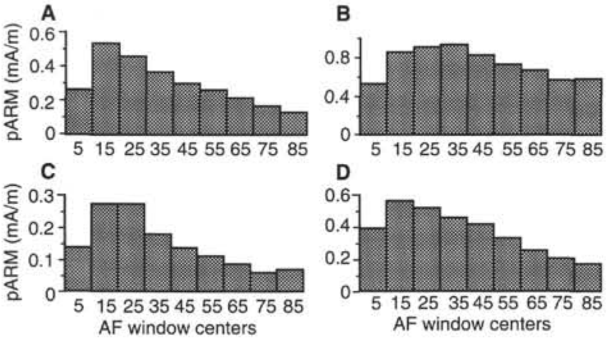

Figure 27. Acquisition of pARM at Site 996. **A.** Sample 164-996A-1H-5, 41–43 cm (3.21 mbsf). **B.** Sample 164-996A-2H-1, 39–41 (8.9 mbsf). **C.** Sample 164-996E-1H-1, 53–55 cm (0.54 mbsf). **D.** Sample 164-996E-7H-5, 81–83 cm (56.5 mbsf).

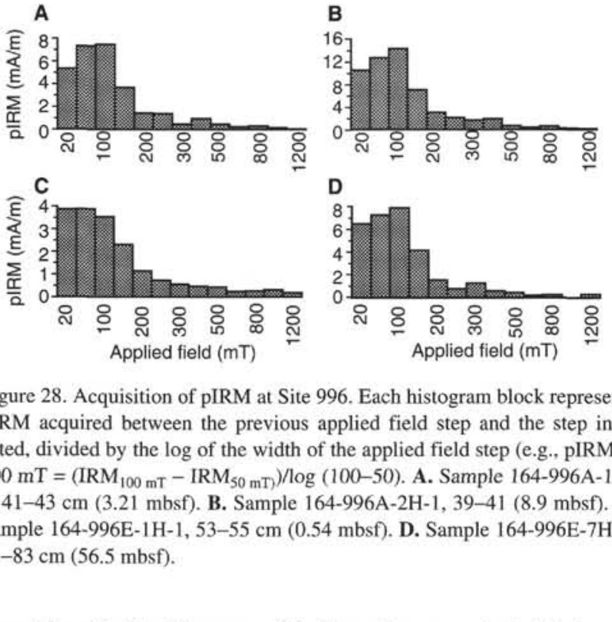

Figure 28. Acquisition of pIRM at Site 996. Each histogram block represents pIRM acquired between the previous applied field step and the step indicated, divided by the log of the width of the applied field step (e.g., pIRM at 100 mT = $(\mathrm{IRM}_{100\ \mathrm{mT}} - \mathrm{IRM}_{50\ \mathrm{mT}})/\log(100–50)$. **A.** Sample 164-996A-1H-5, 41–43 cm (3.21 mbsf). **B.** Sample 164-996A-2H-1, 39–41 (8.9 mbsf). **C.** Sample 164-996E-1H-1, 53–55 cm (0.54 mbsf). **D.** Sample 164-996E-7H-5, 81–83 cm (56.5 mbsf).

cannot be calculated because of the low nitrogen content. Most sediment has a total sulfur content higher than TOC content, which suggests high inorganic sulfur content.

Discussion

The depth profile of headspace gas at Hole 996E is different than that at Holes 996A, 996C, and 996D (Fig. 33). There is a depletion of C_1 in the uppermost 4 m at Hole 996E. This depletion likely reflects oxidation of C_1 in the sulfate reduction zone (see "Inorganic Geochemistry" section, this chapter).

Sediment in all holes contains elevated amounts of higher molecular weight hydrocarbons. In contrast, sediment from Sites 994, 995, and 997 only reach comparable concentrations of these hydrocarbons at a depth below 550 mbsf (see "Organic Geochemistry" sections, "Site 994," "Site 995," and "Site 997" chapters, this volume). Moreover, the TOC content in sediment at Site 996 is too low to produce the necessary amount of methane required to form abundant gas hydrate (see "Gas Hydrate" section, this chapter; Paull, et al., 1994). These observations suggest migration of hydrocarbons from depth.

INORGANIC GEOCHEMISTRY

Thirty whole-round samples were taken for interstitial-water analyses from Holes 996A (nine samples), 996B (one sample), 996C (one sample), 996D (six samples), and 996E (13 samples). These samples (Table 12) span the sedimentary sequence at Site 996 with a frequency of about one sample every 2 m, but they do not include the interval between 13 and 23 mbsf, where poor core recovery occurred.

Samples also were collected and stabilized for shore-based determination of total dissolved sulfide (Cline, 1969). Precipitation of Ag_2S during Cl^- titration suggests that sulfide concentrations are on the order of 1–10 μM.

Chloride

The high-resolution interstitial-water Cl^- profile shows that Cl^- concentration increases from 560–561 mM in the shallowest samples to a maximum of 997 mM at the bottom of Hole 996E (58 mbsf; Fig. 34). In Hole 996E, a distinct increase in Cl^- concentrations and a subtle shift in the Cl^- gradient occur across the zone of low recovery (13–23 mbsf). Several samples from Holes 996A and 996D exhibit low Cl^- values when compared with the trend from Hole 996E. The shallowest samples at Holes 996A, 996C, and 996E contain Cl^- concentrations ~25% higher than depth-coincident samples at Holes 996A and 996D, and they are more similar to values found at all holes at ~20 to 30 mbsf.

Sulfate

Sulfate is depleted at shallow depths in all holes (Fig. 34). Only the shallowest samples at Holes 996A (0.85 mbsf), 996C (1.66 mbsf), and 996D (0.10 mbsf), contain concentrations of SO_4^{2-} that are significantly higher than background levels. Sulfate is depleted above 3.32 mbsf in Hole 996B and between 3.72 and 6.95 mbsf in Hole 996E. The presence of SO_4^{2-} at 10 mbsf in Hole 996A may represent seawater contamination (Table 12).

Alkalinity

Alkalinity in interstitial-water samples from Site 996 is anomalously high at shallow depths (Fig. 34). The two shallowest samples from Hole 996D (0.10 and 0.30 mbsf) and the two samples from Holes 996B and 996C (3.3 and 1.7 mbsf) have alkalinities between 35.7 and 42.2 mM. Such alkalinity values are found at ~100 mbsf at Sites 994 and 995 (see "Inorganic Geochemistry" sections, "Site 994" and "Site 995" chapters, this volume). Dissolved sulfide may constitute a significant proportion of the alkalinity in shallow samples. Alkalinity in Hole 996E increases with depth to a subsurface maximum of 28.7 mM at the base of the SO_4^{2-} reduction zone (6.95 mbsf), decreases to a local minimum just below the zone of low recovery, and increases to 25.1 mM at maximum depth (61.55 mbsf; Fig. 34).

Ammonium

Ammonium generally increases with depth and reaches a maximum ~15 mM in Hole 996E (57.73 mbsf; Fig. 34). Ammonium concentrations are depth dependent rather than hole dependent. When normalized with respect to chloride, the data from all holes plot along the same general trend (Fig. 35).

Table 6. Description of PCS deployment at Site 996.

Core	Depth (mbsf)	Pressure Expected (psig)	Pressure Observed (psig)	Pressure Hydrostatic (%)	Cutting shoe	Core recovered (cm)	Manifold design	Total gas released (mL)
164-996A- 7P	47.5	3253	3328	102	Push-in	0.20	PCS-M4	5415
164-996D- 7P	51.2	3259	2974	91	Push-in	0.00*	PCS-M4	8100
164-996E- 8P	61.3	3273	944	29	Push-in	0.00	PCS-M4	575

Notes: The water depth at Holes 996A, 996D, and 996E is 2170 m. Expected pressure is the hydrostatic pressure, assuming a pressure gradient of 1.467 psi/m. Observed pressure is that first recorded at the PCS sampling station. * = although no core was observed, there must have been a core recovered to release 8100 mL of gas (see text).

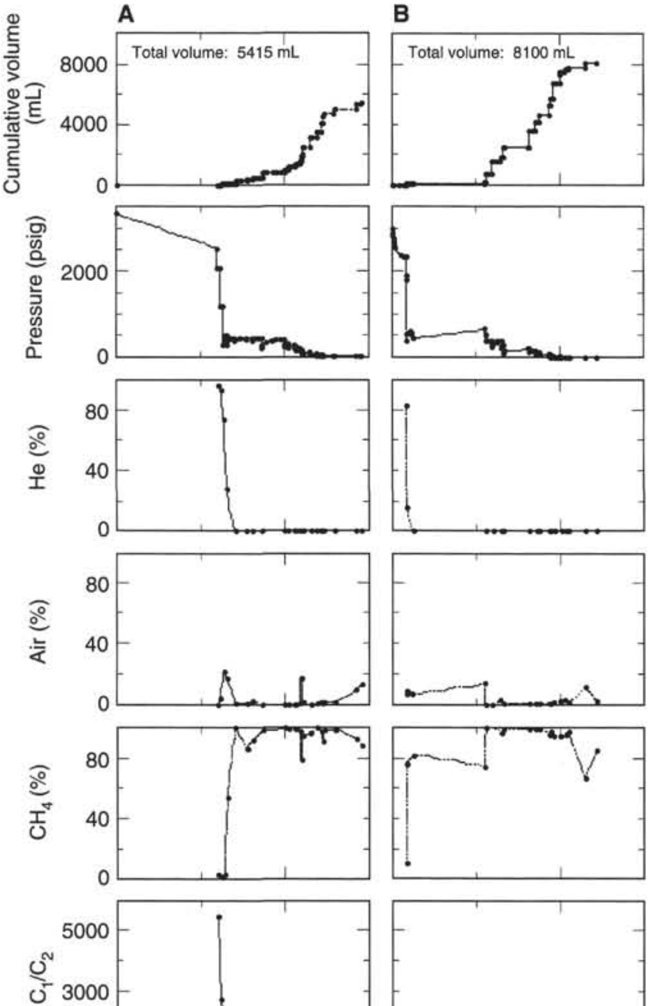

Figures 29. Time-pressure-volume plots and gas compositions of (**A**) Core 164-996A-7P and (**B**) Core 164-996D-7P. The volume represents the cumulative gas volume collected in the manifold bubbling chamber (see "Explanatory Notes" chapter, this volume). The amount of air is determined by adding the concentrations of N_2 and O_2; the amount of He is estimated from the volumes of CH_4 and air.

Potassium

Potassium generally increases with depth, but the shallowest samples from cores within the pockmark have values similar to samples from ~20 to 30 mbsf outside of the pockmark (Fig. 34). The maximum concentration is ~23 mM in Hole 996E (57.73 mbsf). This value is the highest K^+ concentration observed during Leg 164. A few samples from Holes 996A and 996D contain low concentrations of K^+ when compared to the Hole 996E trend below the zone of low recovery. These samples also have low Cl^- concentrations (Fig. 34).

Sodium

The concentrations of Na^+ generally parallel Cl^- concentrations and increase with depth (Fig. 34). The shallowest samples from Holes 996A, 996B, and 996C have Na^+ values that are similar to those observed at ~20 mbsf. Also, there is a distinct increase in the Na/Cl ratio with increasing depth (Fig. 35).

Calcium, Magnesium, and Strontium

Calcium levels in the shallowest samples from Holes 996A, 996B, 996C, and 996D are anomalously low relative to open-marine settings. In Hole 996E, Ca^{2+} decreases to the base of the sulfate reduction zone, reaches a minimum at ~12 mbsf, and increases slightly below the zone of low recovery (Fig. 34). Below ~40 mbsf, samples from Holes 996A, 996D, and 996E have similar Ca/Cl ratios (Fig. 35).

Concentrations of Mg^{2+} decrease to ~30 mM below 30 mbsf and increase to 40 mM at maximum depth within all the holes (Fig. 34). When normalized with respect to Cl^-, all samples plot along a general trend that reaches a constant value of 0.04 below 40 mbsf (Fig. 35).

Concentrations of Sr^{2+} are unusually low in the shallowest samples from Holes 996A, 996C, and 996D. Sr^{2+} generally increases with depth in samples from all the holes (Fig. 34). Minimum Sr^{2+} levels of 30 µM occur near the seafloor (Hole 996D), whereas maximum Sr^{2+} levels of ~290 µM (Hole 996E) are reached at total depth. Samples from all holes plot along the same Sr/Cl trend, which reaches a maximum concentration at ~40 mbsf (Fig. 35).

Dissolved Silica

Dissolved silica increases from ~100 µM near the seafloor to >400 µM at 10 mbsf. Silica then varies from 450 to 650 µM below 25 mbsf (Fig. 34).

Preliminary Interpretations

Source of Salts

Increasing Cl^- and Na^+ concentrations with depth could result from a number of causes (see "Inorganic Geochemistry" section,

Table 7. Gas composition of samples from the PCS at Site 996.

Core	Sample, analysis	Split volume (mL)	C_1 (ppmv)	C_2 (ppmv)	C_3 (ppmv)	i-C_4 (ppmv)	n-C_4 (ppmv)	i-C_5 (ppmv)	n-C_5 (ppmv)	i-C_6 (ppmv)	n-C_6 (ppmv)	n-C_7 (ppmv)	C_1/C_2	C_1/C_{2+}	N_2 (vol%)	O_2 (vol%)	CO_2 (ppmv)
164-996A-																	
7P	G_1-N	10	32,300	6	0.3	0.4				0.3		0.8	5,475	4,195	0.1	0.2	1,700
7P	G_2-N	20	9,900	4	0.2	0.4				0.2		2.2	2,750	1,500	1.1	3.6	1,400
7P	G_3-N	35	31,300	14	0.4	1.5	0.4	0.1					2,285	1,944	18	4.5	1,500
7P	G_4-N	45	542,500	322	8.2	6.5	1.7	1.3		0.1		2.0	1,686	1,588	14	3.2	700
7P	G_5-N	175	1,001,600	644	13.6	5.4	1.2	3.1	0.4	0.4		1.0	1,556	1,498	0.8	0.3	200
7P	G_6-N	90	864,000	590	13.6	4.4	1.0	3.0		1.8		1.5	1,464	1,404	0.6	0.3	1,300
7P	G_7-N	100	921,100	574	12.6	4.7	1.2	3.5				1.6	1,604	1,541	2	0.6	400
7P	G_8-N	300	986,000	678	13.0	4.9	1.2	3.7	0.1			1.4	1,455	1,404	0.1	0.1	200
7P	G_9-N	265	1,000,400	664	13.8	4.8	1.4	4.2		0.4		1.5	1,508	1,451	0.1	0	300
7P	G_{10}-N	180	997,000	681	12.4	4.5	1.2	4.2		0.2		1.5	1,465	1,415	0.1	0	300

Notes: Gas samples taken from the PCS are designated (e.g., G_1) in the order in which they were collected (see Fig. 26, "Site 995" chapter, this volume). Letters following the sample number refer to the shipboard analytical instrument used for gas analyses: G = GC3, and N = NGA (see "Organic Geochemistry" section, "Explanatory Notes" chapter, this volume). Split volume is the total volume of gas from which the sample was taken.

Only part of this table is produced here. The entire table appears on the CD-ROM (back pocket).

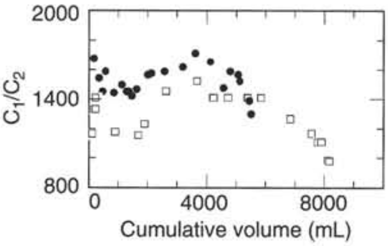

Figure 30. Changes in the C_1/C_2 ratio with respect to cumulative gas volume. Solid circles = Core 164-996A-7P; open squares = Core 164-996D-7P.

"Sites 991/992/993" chapter, this volume). However, the systematic increase in the Na/Cl ratio with depth (Fig. 35) strongly suggests the dissolution of underlying evaporites. Because dissociation of abundant gas hydrate dilutes pore-water samples, a plot of Na/Cl vs. Cl (see "Inorganic Geochemistry, "Sites 991/992/993" chapter, this volume) cannot be used at Site 996.

Advection of Methane

Rapid SO_4^{2-} depletion (Holes 996A, 996B, 996C, and 996D (Fig. 34), high concentrations of interstitial CH_4 (see "Organic Geochemistry" section, this chapter), low amounts of sedimentary organic matter (see "Organic Geochemistry" section, this chapter), and inferred levels of interstitial ΣHS^- indicate that anaerobic methane oxidation ($CH_4 + SO_4^{2-} \rightarrow HS^- + HCO_3^- + H_2O$; Reeburgh, 1976) is a dominant process at Site 996. Complete depletion of SO_4^{2-} within the upper 10 cm (Hole 996D) rarely has been observed in open-ocean sediments. Given the low levels of sedimentary organic matter, the observation is consistent with advective transport of CH_4. Indeed, upward advection of CH_4 drives the chemosynthetic community on the seafloor at the Blake Ridge Diapir.

Carbonate Precipitation

Intense microbial oxidation of CH_4 produces high alkalinity, in particular high bicarbonate concentrations. These conditions promote carbonate precipitation, as indicated by the low Ca^{2+} and Sr^{2+} concentrations immediately below the sediment/water interface. Also, Mg^{2+} concentrations are ~10% less than seawater, suggesting Mg^{2+} uptake into carbonate.

Hydrological Conditions

The presence of chemosynthetic mussel beds, high CH_4 concentrations, and rapid SO_4^{2-} depletion are indicative of upward vertical transport of methane-rich fluids. Interstitial waters in shallow sediment beneath the mussel bed (1.7–3.6 mbsf) provide additional evidence for fault-associated flow. Concentrations of Cl^-, K^+, and Na^+ are significantly higher than expected from depth trends (Fig. 34). This suggests that these waters are derived from depth.

Indurated carbonate layers are concentrated in two depth zones at Site 996 (see "Operations" section, this chapter). Breaks in the downhole trends of Cl^-, alkalinity, NH_4^+, and Na^+, occur across part of the upper depth zones (~15 to 20 mbsf). These breaks in interstitial chemistry may result from gas hydrate dissociation or focused fluid flow along the relatively impermeable carbonate layers. In either case, the carbonate layers likely complicate subsurface fluid flow.

PHYSICAL PROPERTIES

Both whole-round and split sections of cores recovered at Site 996 were tested for physical properties. All undisturbed unsplit sections were analyzed for GRAPE wet bulk density, magnetic susceptibility, and NGR activity on the MST. *P*-wave data were collected with the PWL on the MST, but in most cases only the velocity of the core liner was recorded. *P*-wave velocities also were measured at discrete intervals in split sections using the DSV. Index properties were determined from samples collected from undisturbed split cores. A pocket penetrometer and the vane shear apparatus were used to measure compressive strength and undrained shear strength, respectively. The thermal conductivity of the sediments was measured at one position in each section. Some physical properties tests could not be performed on some of the recovered core sections because of gas expansion, coring and drilling disturbance, the breakdown of gas hydrate, and sampling of hydrate from cores immediately after recovery.

Of the five holes at Site 996, only Hole 996E had sufficient core recovery to make a characterization of downhole physical properties possible. Index properties, thermal conductivity, strength, and DSV

Table 8. Composition of headspace gas in sediment from Site 996.

Core, section	Depth (mbsf)	CO_2 (ppmv)	C_1 (ppmv)	C_2 (ppmv)	C_3 (ppmv)	i-C_4 (ppmv)	n-C_4 (ppmv)	i-C_5 (ppmv)	n-C_5 (ppmv)	i-C_6 (ppmv)	n-C_6 (ppmv)	C_1/C_2	C_1/C_{2+}	CO_2 (µL/kg wet sediment)	C_1 (µL/kg wet sediment)	C_2 (µL/kg wet sediment)	C_3 (µL/kg wet sediment)
164-996A-																	
1H-2	0.90	NA	8,540	8.4	1.5	NA	NA	NA	NA	NA	NA	1,020	863	NA	6,300	6	1
2H-1	8.50	NA	6,810	6.0		NA	NA	NA	NA	NA	NA	1,140	1,140	NA	8,000	7	0
3X-1	10.06	NA	4,510	4.0		NA	NA	NA	NA	NA	NA	1,130	1,130	NA	6,200	6	0
4X-CC	19.00	11,400	3,440	0.8	1.0	1.7		0.5			0.2	4,240	822	39,400	11,900	3	3
8H-3	49.83	NA	820	0.7	0.7	0.6	0.4	0.7	0.1	0.1	0.1	1,230	301	NA	2,900	0	2
9H-2	59.43	NA	10,980	9.4	4.3	3.3	1.4	7.6	1.3	0.8	0.7	1,170	381	NA	44,800	38	18
164-996C-																	
1H-2	1.14	NA	2,060	1.2	1.6	1.4	0.2	3.0			0.1	1,720	276	NA	15,600	9	12
164-996D-																	
1H-1	0.00	NA	4,840	3.6		NA	NA	NA	NA	NA	NA	1,350	1,350	NA	2,700	2	
4H-6	27.24	NA	3,880	2.1		NA	NA	NA	NA	NA	NA	1,850	1,850	NA	12,500	7	
6H-2	42.47	29,000	2,760	2.3	1.6	1.6	0.9	5.4	0.8	0.6	0.4	1,200	203	137,400	13,100	11	8
164-996E-																	
1H-2	1.50	4,500	30.7											13,600	100		
2H-2	5.60	5,100	27,200	3.9	2.4							6,980	4,320	10,400	55,400	8	5
2H-4	8.60	NA	30,800	26.1		NA	NA	NA	NA	NA	NA	1,180	1,180	NA	26,400	22	
2H-6	11.27	NA	190			NA	NA	NA	NA	NA	NA			NA	200		
4H-3	25.40	17,600	6,550	3.1	1.0	0.2	0.2	0.1	0.1	0.1	0.2	2,110	1,330	37,300	13,900	7	2
5H-3	34.29	32,000	6,650	3.5	0.9	0.3	0.1	0.3	0.1		0.1	1,900	1,260	67,900	14,100	7	2
6X-4	42.20	NA	13,300	13.2		NA	NA	NA	NA	NA	NA	1,000	1,010	NA	28,200	28	
7H-4	51.80	NA	9,220	9.4		NA	NA	NA	NA	NA	NA	980	980	NA	33,700	34	

Notes: C_1 through C_6 = the alkanes: methane, ethane, propane, butane, pentane, and hexane. Iso- and normal configurations of butane, pentane, and hexane are designated with *i*- and *n*- prefixes. C_1/C_2 = the methane/ethane ratio, and C_1/C_{2+} = ratio of methane/Σ (C_2 through C_6). NA = not analyzed.

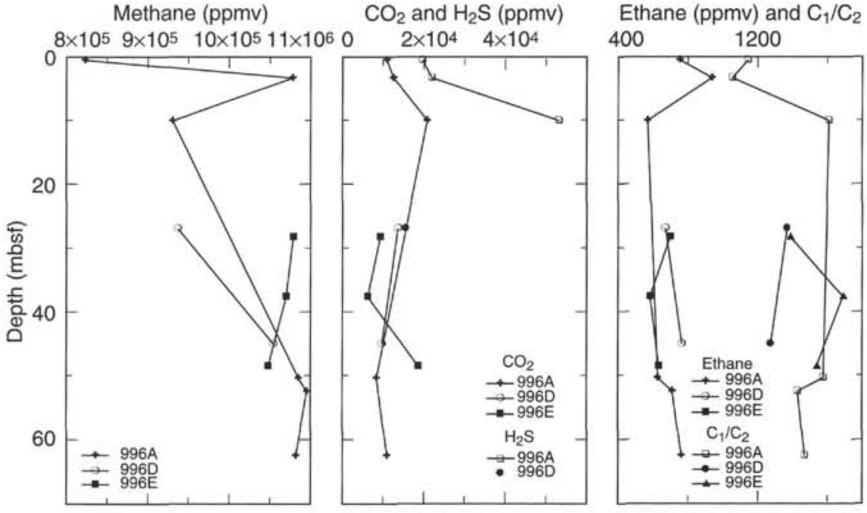

Figure 31. C_1, H_2S, CO_2, and C_2 concentrations and C_1/C_2 ratios in free gas of sediment from Holes 996A, 996D, and 996E.

Table 9. Composition of free gas collected in syringes from sediments at Site 996.

Core, section	Depth (mbsf)	O_2 (ppmv)	N_2 (ppmv)	CO_2 (ppmv)	H_2S (ppmv)	C_1 (ppmv)	C_2 (ppmv)	C_3 (ppmv)	i-C_4 (ppmv)	n-C_4 (ppmv)	i-C_5 (ppmv)	n-C_5 (ppmv)	i-C_6 (ppmv)	n-C_6 (ppmv)	n-C_7 (ppmv)	C_1/C_2	C_1/C_{2+}
164-996A-																	
1H-1	0.51	27,000	110,000	10,900	19,600	861,400	753	24.7	8.5	2.4	9.7	1.4				1,140	1,080
1H-5	3.30	2,000	1,000	12,500	21,900	989,000	937	18.0	7.0		9.0					1,060	1,020
3X-1	10.01	7,000	54,000	20,800	53,200	915,400	569	17.1	2.1	0.6	0.3			0.3		1,610	1,550
8H-3	50.34	9,000	31,000	8,400		992,600	629	28.2	11.1	2.5	7.5	1.2	0.6	0.4		1,580	1,460
8H-5	52.44	3,000	5,000			997,700	697	19.5	4.5	1.0	3.2	0.6	0.2	0.1		1,430	1,370
9H-5	62.45	3,000	2,000	10,900		1,076,000	733	24.7	8.6	2.1	7.2	1.0	0.4	0.2		1,470	1,390
164-996D-																	
4H-5	26.87	2,000	5,000	13,600	15,500	918,400	671	6.1	1.7	0.6	2.5	1.0	0.1	0.2		1,370	1,340
6H-4	45.00	1,000	1,000	9,700		977,200	766	22.0	5.5	1.9	8.0	1.2	1.0	0.7		1,280	1,210
164-996E-																	
4H-5	28.21	2,000	2,000	9,300		989,300	714	11.0	1.1	0.5	1.6	0.3	0.2	0.2		1,390	1,360
5H-5	37.56	2,000	5,000	6,200		985,000	583	10.0	2.4	0.8	2.4	0.5	0.2	0.2	0.8	1,690	1,640
7X-5	48.51	1,000	1,000	18,600		974,000	633	20.3	6.2	1.6	5.9	0.6	0.8			1,540	1,460

Notes: Oxygen (O_2) and nitrogen (N_2) concentrations are included as a guide to the amount of air contamination in each sample. C_1 through C_7 = the alkanes: methane, ethane, propane, butane, pentane, hexane, and heptane. Iso- and normal configurations of butane, pentane, and hexane are designated with *i*- and *n*- prefixes. C_1/C_2 = the methane/ethane ratio, and C_1/C_{2+} = the ratio methane/Σ (C_2 through C_6).

Table 10. Composition of gas collected in gas-collection chambers at Site 996.

Core, section	Sample	Depth (mbsf)	O_2 (ppmv)	N_2 (ppmv)	C_1 (ppmv)	CO_2 (ppmv)	C_2 (ppmv)	C_3 (ppmv)	i-C_4 (ppmv)	n-C_4 (ppmv)	i-C_5 (ppmv)	n-C_5 (ppmv)	i-C_6 (ppmv)	n-C_6 (ppmv)	C_1/C_2	C_1/C_{2+}
164-996A-																
1H-3	1	2.30	NA	NA	8,500	NA	8	1.5							1,020	863
1H-3	1	2.30	183,000	748,000	8,300	1,000		1.5								5,540
8H-4	1	50.93	149,000	613,000	238,800	3,100	124	3.9	1.4	0.4	1.0	0.4	0.1		1,930	1,820
8H-4	2	50.93	62,000	259,000	671,000		287	9.4	3.1	0.7	2.4	0.6	0.2	0.1	2,340	2,210
8H-4	3	50.93	56,000	228,000	661,400	8,000	271	8.8	3.0	0.7	3.0				2,440	2,310
8H-4	3	50.93	65,000	254,000	671,200	7,500	263	7.0	2.5	0.5	1.4	1.0	0.3		2,550	2,440
9H-3	1	61.26	76,000	314,000	597,500	6,300	433	9.2	3.3	0.8	3.4	0.8	0.3		1,380	1,330
164-996D-																
4H-1	1	23.18	152,000	661,000	170,500	5,000	119	2.4	1.6	0.4	1.3	0.7	0.2		1,430	1,360
4H-1	2	23.18	66,000	275,000	647,200	6,800	462	10.8	4.1	1.0	4.0	1.0	0.4		1,400	1,340
6H-1	1	42.28	126,000	519,000	345,200		262	8.6	2.1	0.6	2.2	0.5	0.2		1,320	1,250
6H-2	1	43.05	88,000	365,000	535,300	5,700	397	8.0	2.8	0.8	2.9	1.0	0.3		1,350	1,300
9H-4	1	46.05	177,000	734,000	73,800	2,200	51	1.8	1.1		1.2	1.1	0.3		1,450	1,300
9H-6	1	49.05	147,000	616,000	221,300	5,100	158	4.5	2.5	0.3	2.5	1.2	0.6	0.4	1,400	1,300

Notes: Oxygen (O_2) and nitrogen (N_2) concentrations are included as a guide to the amount of air contamination in each sample. C_1 through C_7 = the alkanes: methane, ethane, propane, butane, pentane, hexane, and heptane. Iso- and normal configurations of butane, pentane, and hexane are designated with *i*- and *n*- prefixes. C_1/C_2 = the methane/ethane ratio, and C_1/C_{2+} = the ratio methane/Σ (C_2 through C_6). NA = not analyzed.

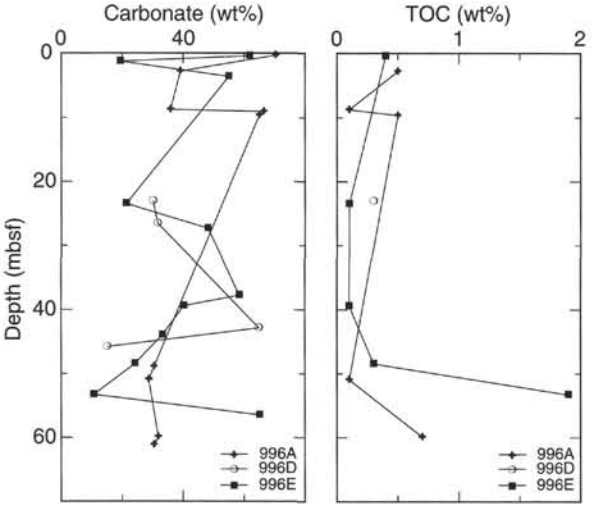

Figure 32. Calcium carbonate and total organic carbon content vs. depth in sediment from Holes 996A, 996D, and 996E.

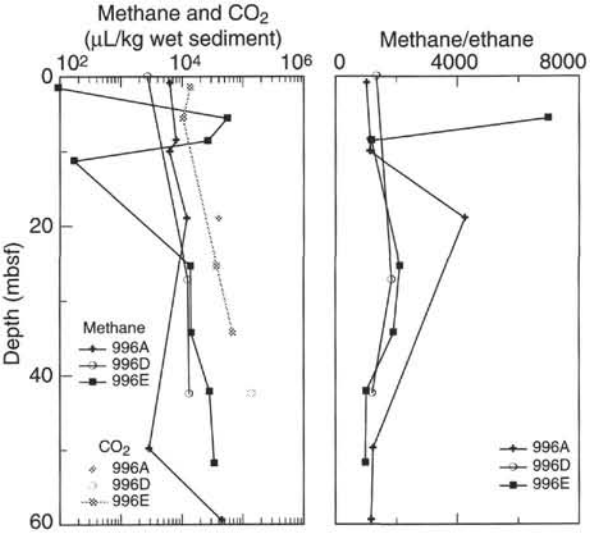

Figure 33. C_1 and CO_2 concentrations and C_1/C_2 ratios vs. depth in headspace gas of sediment from Holes 996A, 996D, and 996E.

Table 11. Carbonate, carbon, nitrogen, and sulfur contents in sediment from Site 996.

Core, section, interval (cm)	Depth (mbsf)	$CaCO_3$ (wt%)	Organic carbon (wt%)	Total nitrogen (wt%)	Total sulfur (wt%)
164-996A-					
1H-1, 33–35	0.33	61.6	NA	NA	NA
1H-5, 3–4	2.82	34.2	0.5	0.0	0.4
2H-1, 27–28	8.77	31.4	0.1	0.0	0.4
2H-CC, 9–10	9.08	58.2	NA	NA	NA
3X-1, 14–15	9.64	56.9	0.5	0.1	0.6
8H-1, 40–41	48.90	26.7	NA	NA	NA
8H-4, 50–51	50.93	25.2	0.1	0.0	0.8
9H-2, 45–46	59.88	27.9	0.7	0.1	1.0
9H-3, 45–46	61.13	26.7	NA	NA	NA
164-996B-					
1H-3, 37–38	2.34	21.4	0.4	0.0	0.6
1H-4, 33–34	2.92	51.6	NA	NA	NA
164-996C-					
1H-3, 21–22	2.12	35.8	0.4	0.1	0.8
164-996D-					
4H-1, 45–46	23.05	26.4	0.3	0.0	1.1
4H-5, 20–21	26.56	27.7	NA	NA	NA
6H-2, 40–41	42.87	56.8	NA	NA	NA
6H-5, 60–61	45.81	13.3	NA	NA	NA
164-996E-					
1H-1, 43–44	0.43	54.1	0.4	0.1	0.1
1H-1, 128–129	1.28	17.0	NA	NA	NA
1H-3, 65–66	3.65	48.1	NA	NA	NA
4H-1, 27–28	23.47	18.7	0.1	0.1	1.5
4H-4, 45–46	27.35	42.1	NA	NA	NA
5H-5, 73–74	37.78	51.2	NA	NA	NA
5H-7, 44–45	39.41	35.2	0.1	0.0	0.7
6X-2, 44–45	43.95	29.1	NA	NA	NA
6X-5, 44–45	48.45	21.2	0.3	0.1	0.7
7H-2, 63–64	53.29	9.4	1.9	0.1	1.4
7H-5, 79–80	56.47	57.0	NA	NA	NA

Note: NA = not analyzed.

data for all holes are available on CD-ROM (back pocket). Selected index properties for all holes are reported in Table 13.

Index Properties

Wet bulk density, porosity, and grain density (Fig. 36) determined from index properties measurements are nearly constant as a function of depth in Hole 996E. Wet bulk density averages 1.69 g/cm^3, with the minimum value of 1.48 g/cm^3 occurring just below the seafloor. Except in the upper 5 m of the hole, the wet bulk density values obtained using gravimetric methods correlate well with the high-resolution GRAPE data. Both GRAPE and index properties data indicate a decrease in wet bulk density between 39 and 42 mbsf and an increase in wet bulk density with depth starting at 43–45 mbsf.

Water contents measured using both wet and dry methods show a gradual change as a function of depth, with values decreasing from 51% to 31% (wet) and 103% to 44% (dry) in the uppermost 12 m of the hole. Water content is relatively constant deeper than 23 mbsf.

Porosity values decrease from 73% near the seafloor to an average of 63% at the bottom of the hole. Grain density obtained using the dry method barely deviates from an average value of 2.72 ± 0.1 g/cm^3 as a function of depth.

Acoustic Velocity

P-wave velocities were measured with the PWL on whole-round sections recovered in Hole 996E, but almost no reliable data were obtained. Even the few data that lie between 1.45 and 1.65 km/s are too scattered to delineate any general trend. *P*-wave velocities were measured with the DSV apparatus at only six locations over an interval of 1.5 m in Hole 996E, and the data do not correlate well with the PWL values obtained at the same depths.

Undrained Shear Strength

Undrained shear strength values obtained with a pocket penetrometer and the vane shear apparatus vary from 12.3 to 61.3 kPa and from 10.3 to 45.7 kPa, respectively. Strength is nearly constant between 4 and 12 mbsf and increases linearly between 25 and 37 mbsf. Average strength decreases slightly between 37 and 52 mbsf.

Natural Gamma Radiation

NGR values range from 10 to 25 cps at depths shallower than 50 mbsf, but the peaks decrease in amplitude at depths greater than 50 mbsf. The most pronounced NGR anomaly is centered at 48.5 mbsf.

Table 12. Interstitial-water data for Site 996.

Core, section, interval (cm)	Depth (mbsf)	pH	Alk (mM)	Sal (g/kg)	Cl$^-$ (mM)	Mg^{2+} (mM)	Ca^{2+} (mM)	SO$_4^{2-}$ (mM)	NH$_4^+$ (µM)	SiO$_2$ (µM)	K$^+$ (mM)	Sr^{2+} (µM)	Na$^+$ (mM)
164-996A-													
1H-1, 85–95	0.85	8.45	21.5	34.0	561	50.4	3.9	7.2	0	112	12.2	42	478
1H-6, 33–38	3.62	8.25	23.6	41.0	693	53.6	1.9	0.3	980	312	16.4	63	584
3X-1, 61–71	10.11	8.52	26.7	36.0	608	41.6	4.2	1.3	1,520	465	13.4	144	525
8H-1, 96–111	49.46	7.73	28.9	44.0	952	42.8	4.2	0.1	14,590	480	22.7	248	848
8H-2, 0–12	49.61	7.40	29.7	55.0	959	44.1	5.0	0.0	14,930	546	21.7	261	866
8H-5, 19–34	52.12	7.68	27.6	53.0	933	41.4	3.8	0.0	14,510	480	23.1	235	845
8H-5, 72–82	52.65	7.38	26.6	49.0	852	39.0	4.1	0.0	13,900	431	21.0	222	793
9H-1, 80–90	58.80	7.62	26.5	50.0	907	39.1	4.1	0.9	14,420	459	21.7	228	809
9H-3, 87–102	61.55	7.67	25.2	47.0	840	36.5	3.8	0.0	12,310	461	19.5	218	762
164-996B-													
1H-3, 135–150	3.32	8.40	35.7	40.0	675	54.2	3.2	0.6	970	478	15.2	88	574
164-996C-													
1H-2, 52–67	1.66	8.27	42.2	42.0	701	61.3	3.4	1.9	540	202	14.8	49	584
164-996D-													
1H-1, 0–20	0.10	8.53	36.3	34.0	572	51.0	2.4	1.4	40	93	12.2	34	487
1H-1, 20–40	0.30	8.47	38.0	34.0	563	49.2	2.4	0.3	30	106	12.4	39	481
4H-2, 10–25	23.87	7.50	17.3	40.0	712	36.7	5.9	0.2	3,740	482	16.3	213	613
4H-7, 140–150	30.14	8.13	16.7	40.0	712	36.3	6.0	0.0	3,640	478	15.7	215	612
6H-2, 52–67	42.99	7.75	21.9	47.0	857	37.0	4.5	0.3	10,720	567	19.9	243	751
6H-5, 28–43	45.49	7.52	18.0	40.5	739	31.8	3.7	0.4	8,710	642	16.6	200	647
164-996E-													
1H-1, 135–150	1.35	8.02	4.2	34.0	560	51.7	10.6	28.1	10	214	12.4	102	480
1H-3, 72–87	3.72	8.61	16.5	35.0	563	50.5	7.6	17.3	250	327	12.6	101	483
2H-2, 135–150	6.95	8.65	28.7	33.5	573	43.9	3.7	0.9	460	412	12.9	114	494
2H-4, 134–150	9.94	8.68	27.7	34.0	580	40.5	4.3	0.6	780	527	13.2	131	502
2H-6, 117–132	12.44	8.58	20.7	34.0	590	40.1	3.1	0.1	1,000	425	13.4	115	505
4H-3, 135–150	26.75	7.77	15.7	46.0	834	33.6	5.2	0.0	9,190	540	18.4	240	737
4H-5, 135–150	29.05	7.51	15.5	44.0	812	31.7	4.7	0.0	8,290	597	17.2	228	706
5H-4, 135–150	36.90	7.32	15.7	46.0	823	32.3	4.8	0.0	7,850	576	18.4	276	739
5H-6, 72–87	38.82	7.29	17.9	48.5	870	34.5	4.8	0.0	10,590	614	19.1	282	782
6X-4, 135–150	47.86	7.85	20.6	52.0	940	37.4	5.3	0.1	11,770	631	20.7	274	843
6X-6, 135–150	50.86	7.39	20.9	52.0	934	37.2	5.4	0.8	12,120	631	20.2	278	837
7H-3, 10–19	54.26	7.75	24.3	54.0	970	38.4	5.0	0.0	14,710	438	22.5	281	869
7H-6, 55–75	57.73	7.85	25.2	56.5	997	40.5	5.1	0.0	15,080	552	23.5	289	910

Notes: Alk = alkalinity, and Sal = salinity. Sodium was analyzed by atomic emission spectroscopy.

Thermal Conductivity

Only 10 thermal conductivity measurements were obtained in cores recovered from Hole 996E. Thermal conductivity values vary from 0.9 to 1.4 W/(m·K), but the data are too sparse to delineate general trends.

Discussion

Because of the paucity of data, the poor core recovery, and the shallow depth of the holes, no physical properties units were delineated at Site 996. Although gas hydrate was recovered from Hole 996E, the laboratory measurements do not reveal marked physical properties changes that can be spatially associated with the occurrence of in situ gas hydrate.

Physical properties data for Hole 996D are complete only for Cores 164-996D-4H and 6H. Water content (wet and dry methods) and porosity data from these cores are much lower than those measured from comparable depths (23–31.5 mbsf and 42.9–47.9 mbsf) in Hole 996E. The inferred lateral variations in sediment physical properties between the two holes, which are separated by only 80 m, are consistent with other observations indicating significant lateral variability at Site 996.

SYNTHESIS AND SIGNIFICANCE

At Site 996 five holes were drilled along an 80-m-long east-west transect across pockmarked seafloor above the Blake Ridge Diapir. VIT camera surveys of the seafloor taken before drilling confirm the presence of mussel beds, which are presumably part of a chemosynthetic community. Holes 995A, 995B, and 995C were located in this mussel bed. Holes 996D and 996E were 40 m to the east and west of the mussel bed, respectively (Fig. 37).

Evidence for Fluid Advection

Both methane and hydrogen sulfide are present in high quantities directly underneath the mussel beds at Site 996. The uppermost one to two cores from Holes 996A, 996B, 996C, and 996D had high H_2S concentrations (>100 ppm) as measured using Pack Rat personal H_2S monitors, which draw gas from the open ends of the core liners. Vacutainer gas analysis showed as much as 53,200 ppmv of H_2S in the gas extracted from the liners of the cores from above 10.01 mbsf (Section 164-996A-3X-1; see "Organic Geochemistry" section, this chapter). Methane concentrations directly under the mussel bed ranged to as much as 15,600 µL/kg wet sediment in headspace Sample 164-996C-1H-2. Both methane and hydrogen sulfide compounds can support chemosynthetic production.

Although the high C_1/C_2 ratio (>1000) of the gas indicates that the methane is predominately of microbial origin, the concentrations exceed amounts that could be produced within these sediments; thus, advection of fluid or gas has to be occurring at this site. Methane concentrations remained high at depth, but the H_2S concentrations decreased below ~20 mbsf, suggesting that H_2S was not being carried along in the advecting fluids. H_2S may have been produced locally via anaerobic methane oxidation (see "Inorganic Geochemistry" section, this chapter).

Gas Hydrate Occurrence

At Site 996, gas hydrate was encountered as massive pieces in the uppermost cores. Below 25 mbsf, gas hydrate occurred as thin platy vein fillings and as cylindrical rods that appeared to have developed

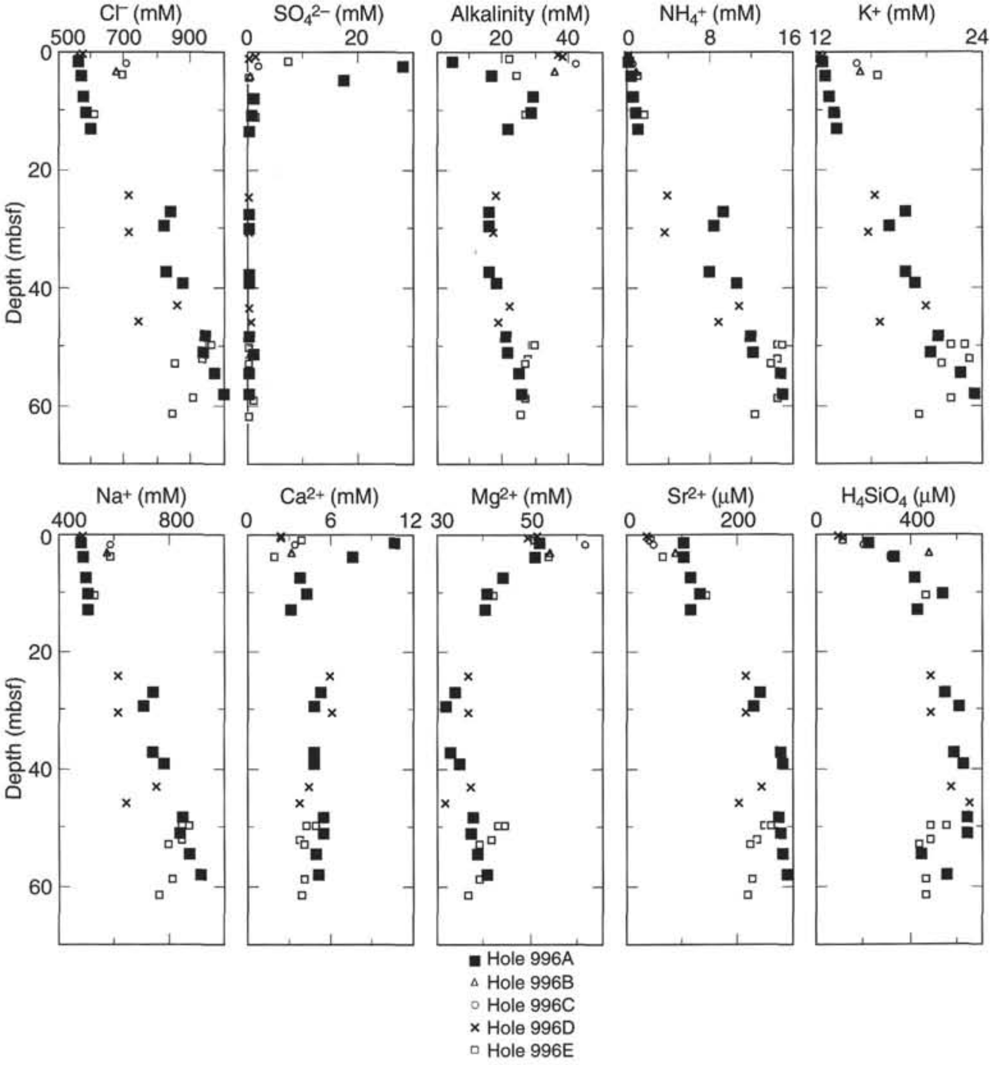

Figure 34. Concentration profiles for various dissolved species in interstitial waters at Site 996. Concentrations have not been corrected for seawater contamination. Sodium was measured by AES.

within sediment burrows. Decomposition experiments indicate that the gas hydrate was dominantly composed of methane (see "Gas Hydrate" section, this chapter).

Association of Gas Hydrate and Pockmarks

The seafloor pockmarks near this site have been attributed to the formation of gas hydrate in the shallow subsurface (Paull et al., 1995). Because gas hydrate is less dense than seawater, massive gas hydrate that develops near the seafloor has the potential of floating off the seafloor. When this happens, the gas hydrate may carry entrapped sediment. Thus, sediment entrapped in the gas hydrate can potentially be transported some distance away by contour currents before the associated gas hydrate decomposes and the sediment drops back to the seafloor. Potential dropstones occur on the seafloor surrounding the pockmark (see Fig. 7D). If this process continues over time, it may result in the excavation of a pockmark. The large pieces of gas hydrate, both pure and with interlayers of sediment, sampled in the uppermost cores demonstrate that appropriate conditions exist at Site 996 for excavation of pockmarks by gas hydrate rafting.

Carbonate Cements and Diagenesis

Indurated diagenetic carbonates were recovered at Site 996, and they probably were responsible for the generally poor core recovery (45% average recovery). Core penetration rates were used to help define the vertical distribution of the indurated carbonates (see Fig. 12). Hard carbonate beds apparently are concentrated in two zones (between 5 and 20 mbsf and between 30 and 50 mbsf; Fig. 37). The upper indurated carbonate zone is 6–12 m thick, and the lower indurated carbonate zone is estimated to be 8–18 m thick. The internal distribution of hard and soft beds within each of these carbonate zones is unknown.

Both carbonate horizons contained carbonate breccias that reveal multiple stages of carbonate cementation. The breccias consist of cemented nannofossil clay intraclasts that are, in turn, cemented by both micritic and fibrous carbonate. In some cases, the remaining space among the carbonate clasts is filled by equant sparry calcite (Fig. 13). Multistage cementation and brecciation of carbonate clasts have been reported from other pockmark carbonates (e.g., Hovland et al., 1987; Matsumoto, 1990). The brecciation and variable fabrics of the carbonates could be explained by (1) buoyant removal of gas hydrate formed near the seafloor, (2) rupturing of carbonate seals caused by accumulations of overpressured gas-bearing fluids beneath indurated carbonate beds, or (3) local faulting.

The uppermost 1 to 2 m of core from Holes 996A, 996B, and 996C was poorly indurated but contained abundant aragonite needles that are apparently authigenic. This same zone also contains small aragonite- and calcite-cemented nodules and cement-coated mussel shell fragments. Sharp decreases in Ca^+, Mg^+, and Sr^- concentrations and the high alkalinity values of interstitial waters within these sediments imply that authigenic carbonates are currently precipitating in this zone.

Biostratigraphic and paleomagnetic data indicate that the lower carbonate layer was deposited in the early Pleistocene. Thus, seepage and chemosynthetic colonization occurred at least intermittently in this area throughout the Pleistocene.

Origin of the Blake Ridge Diapir

The chloride concentrations of interstitial waters from sediments overlying the Blake Ridge Diapir are very high, and the ratios of Cl^- to other ions imply that there is a source of evaporitic salt nearby. Thus, the Blake Ridge Diapir probably is salt cored. Presumably, the salt has come up from near the base of the Carolina Trough, which is ~8 km below the seafloor at this site (see Fig. 3, "Introduction" chapter, this volume).

Source of the Advecting Fluids

The chemosynthetic ecosystem, the high concentrations of reduced inorganic compounds found near the surface (<10 mbsf), the fossil seep deposits, and gas-hydrate-lined veins at greater depth (>10 mbsf) indicate that fluid advection is occurring and has occurred at this site at least intermittently throughout the Quaternary. Thus, the composition of the fluids and gases that were sampled here reveal the composition of the underlying fluids and gases. Two sources for these fluids and/or gases are implicated:

1. The high chloride concentrations of the interstitial waters indicate that at least some of the fluids have been in contact with salt in the core of the diapir.
2. The methane that is arriving at the seafloor at this site is largely microbial, like the gases from Sites 994, 995, and 997. Thus, we infer that the sampled fluids and gases that are venting at Site 996 have been transported upward from the underlying gas-bearing sediment section that slopes up around the diapir (see Fig. 2).

REFERENCES

Cande, S.C., and Kent, D.V., 1995. Revised calibration of the geomagnetic polarity timescale for the Late Cretaceous and Cenozoic. *J. Geophys. Res.,* 100:6093–6095.

Carozzi, A.V., 1989. *Carbonate Rock Depositional Models: A Microfacies Approach:* Englewood Cliffs, NJ (Prentice Hall).

Cline, J.D. 1969. Spectrophotometric determination of hydrogen sulfide in natural waters. *Limnol. Oceanogr.,* 14:454–458.

Davidson, D.W., Leaist, D.G., and Hesse, R., 1983. Oxygen-18 enrichment in the water of a hydrate. *Geochim. Cosmochim. Acta,* 47:2293–2295.

Dillon, W.P., Popenoe, P., Grow, J.A., Klitgord, K.D., Swift, B.A., Paull, C.K., and Cashman, K.V., 1982. Growth faulting and salt diapirism: their relationship and control in the Carolina Trough, Eastern North America. *In* Watkins, J.S., and Drake, C.L. (Eds.), *Studies of Continental Margin Geology.* AAPG Mem., 34:21–46.

Housen, B.A., and Musgrave, R.J., 1996. Rock-magnetic signature of gas hydrates in accretionary prism sediments. *Earth Planet. Sci. Lett.,* 139:509–519.

Hovland, M., and Judd, A.G., 1988. *Seabed Pockmarks and Seepages: Impact on Geology, Biology and the Marine Environment:* London (Graham and Trotman).

Hovland, M., Talbot, M.R., Qvale, H., Olaussen, S., and Aasberg, L., 1987. Methane-related carbonate cements in pockmarks of the North Sea. *J. Sediment. Petrol.,* 57:881–892.

Hutchinson, D.R., Grow, J.A., Klitgord, K.D., and Swift, B.A., 1982. Deep structure and evolution of the Carolina Trough. *In* Watkins, J.S., and Drake, C.L. (Eds.), *Studies of Continental Margin Geology.* AAPG Mem., 34:129–152.

Jorgensen, N.O., 1992. Methane-derived carbonate cementation of marine sediments from the Kattegat, Denmark: geochemical and geological evidence. *Mar. Geol.,* 103:1–13.

MacDonald, I.R., Guinasso, N.L., Jr., Sassen, R., Brooks, J.M., Lee, L., and Scott, K.T., 1994. Gas hydrate that breaches the sea floor on the continental slope of the Gulf of Mexico. *Geology,* 22:699–702.

Matsumoto, R., 1990. Vuggy carbonate crust formed by hydrocarbon seepage on the continental shelf off Baffin Island, northeast Canada. *Geochem. J.,* 24:143–158.

Paull, C.K., Chanton, J.P., Neumann, A.C., Coston, J.A., Martens, C.S., and Showers, W., 1992. Indicators of methane-derived carbonates and chemosynthetic organic carbon deposits: examples from the Florida Escarpment. *Palaios,* 7:361–375.

Paull, C.K., and Dillon, W.P., 1981. Appearance and distribution of the gas hydrate reflector in the Blake Ridge region, offshore southeastern United States. *USGS Misc. Field Studies Map,* 1252.

Paull, C.K., Spiess, F.N., Ussler, W. III, and Borowski, W.A., 1995. Methane-rich plumes on the Carolina Continental Rise: associations with gas hydrates, *Geology,* 23: 89–92.

Paull, C.K., Ussler, W., III, and Borowski, W.S., 1994. Sources of biogenic methane to form marine gas hydrates: in situ production or upward migration? *Ann. N.Y. Acad. Sci.,* 715:392–409.

Paull, C.K., Ussler, W., III, and Dillon, W.P., 1991. Is the extent of glaciation limited by marine gas-hydrates? *Geophys. Res. Lett.,* 18:432–434.

Reeburgh, W.S., 1976. Methane consumption in Cariaco Trench waters and sediments. *Earth Planet. Sci. Lett.,* 28:337–344.

Reeburgh, W.S., 1982. A major sink and flux control for methane in marine sediments: anaerobic consumption. *In* Fanning, K.A., and Manheim, F.T. (Eds.), *The Dynamic Environment of the Ocean Floor:* Lexington, MA (D.C. Heath), 203–207.

Ritger, S., Carson, B., and Suess, E., 1987. Methane-derived authigenic carbonates formed by subduction-induced pore-water expulsion along the Oregon/Washington margin. *Geol. Soc. Am. Bull.,* 98:147–156.

Rowe, M.M., and Gettrust, J.F., 1993. Faulted structure of the bottom-simulating reflector on the Blake Ridge, western North Atlantic. *Geology,* 21:833–836.

Shipboard Scientific Party, 1994. Site 892. *In* Westbrook, G.K., Carson, B., Musgrave, R.J., et al., *Proc. ODP, Init. Repts.,* 146 (Pt. 1): College Station, TX (Ocean Drilling Program), 301–378.

Spiess, F.N., and Tyce, R.C., 1973. *MPL Deep Tow Instrument System.* Scripps Inst. of Oceanogr., Ref. Ser. 73-4.

Tucholke, B.E., and Mountain, G.S., 1979. Seismic stratigraphy, lithostratigraphy, and paleosedimentation patterns in the North Atlantic Basin. *In* Talwani, M., Hay, W., and Ryan, W. (Eds.), *Deep Drilling Results in the Atlantic Ocean: Continental Margins and Paleoenvironment.* Am. Geophys. Union, Maurice Ewing Ser., 3:58–86.

Ms 164IR-109

NOTE: Core-description forms ("barrel sheets") and core photographs can be found in Section 4, beginning on page 337. Forms containing smear-slide data can be found in Section 5, beginning on page 599. Forms containing thin-section data can be found in Section 6, beginning on page 623.

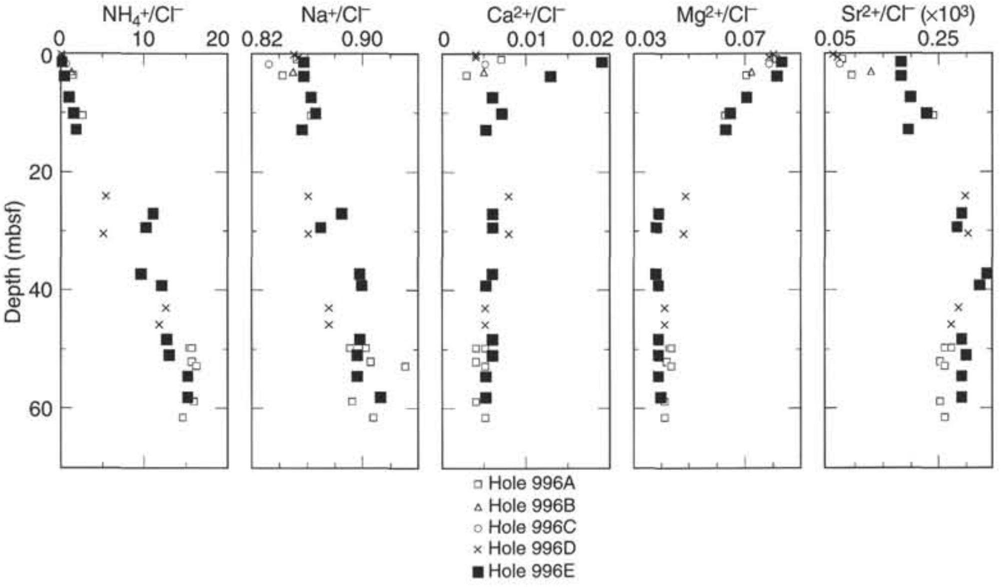

Figure 35. Concentration ratios of selected species in interstitial waters at Site 996. Sodium was measured using AES. The average error in the Na/Cl ratio is 0.006.

Table 13. Index properties of sediment samples from Site 996.

		Water	Water	Density				
Core, section, interval (cm)	Depth (mbsf)	content (wet%)	content (dry%)	Bulk (g/cm³)	Grain (g/cm³)	Dry (g/cm³)	Porosity (%)	Void ratio
164-996A-								
3X-1, 42–44	9.92	31.10	45.14	1.81	2.72	1.25	54.87	1.20
3X-CC, 12–14	10.38	25.05	33.42	1.89	2.79	1.42	46.29	0.91
8H-1, 90–82	49.40	41.57	71.16	1.63	2.69	0.94	65.99	1.87
8H-3, 6–8	49.89	41.05	69.65	1.66	2.74	0.96	66.34	1.86
8H-3, 32–34	50.15	40.12	67.00	1.66	2.68	0.97	65.01	1.75
8H-4, 13–15	50.56	36.75	58.10	1.56	2.71	1.07	55.91	1.54
8H-5, 9–11	52.02	34.09	51.71	1.61	2.71	1.15	53.54	1.37
8H-6, 23–25	53.33	36.94	58.58	1.57	2.67	1.06	56.71	1.53
9H-1, 92–94	58.92	37.53	60.09	1.69	2.74	1.05	61.91	1.61
9H-1, 126–128	59.26	37.12	59.04	1.68	2.72	1.06	60.95	1.57

Only part of this table is produced here. The entire table appears on the CD-ROM (back pocket).

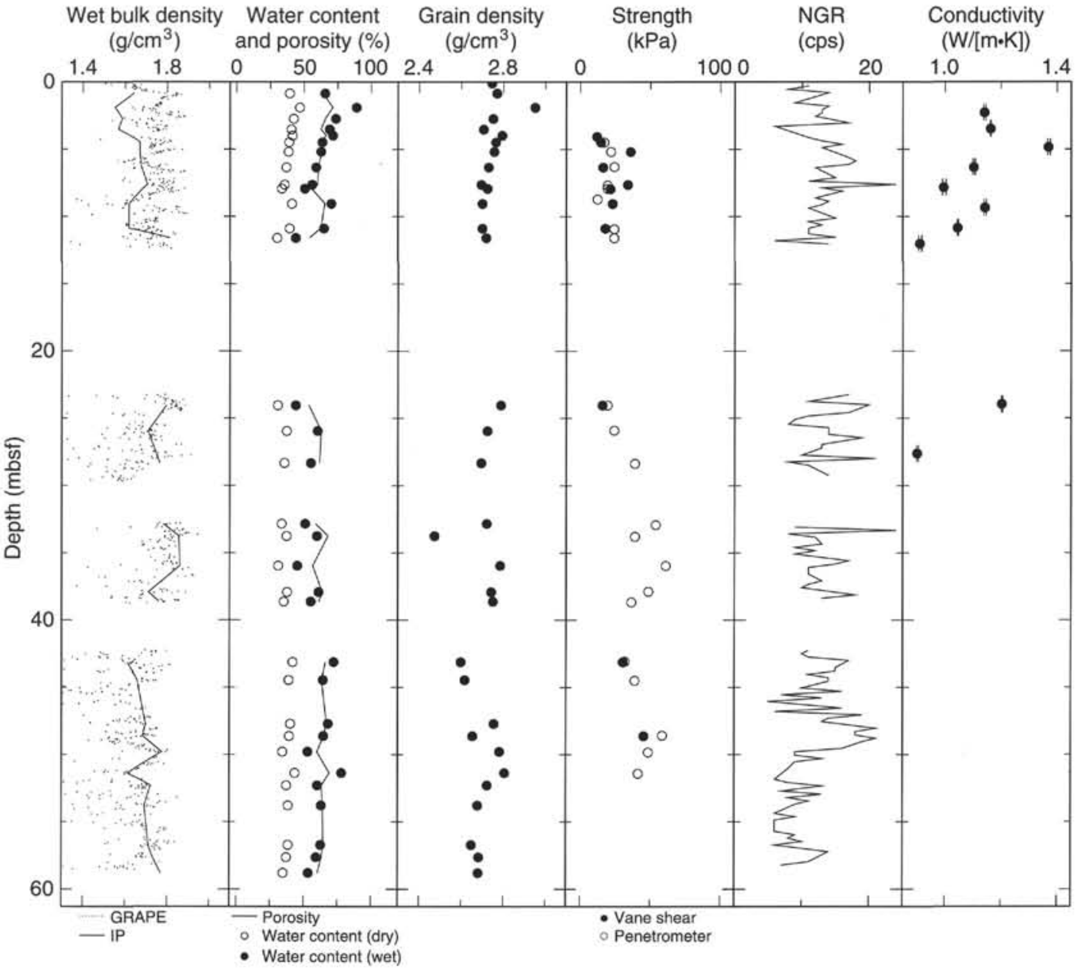

Figure 36. Physical properties data from Hole 996E. IP = index properties data. The grain density data were calculated using the dry method (see "Physical Properties" section, "Explanatory Notes" chapter, this volume. NGR = natural gamma radiation in average counts per second. Error bars indicate analytical uncertainty in the conductivity data. No physical properties units were delineated for Hole 996E.

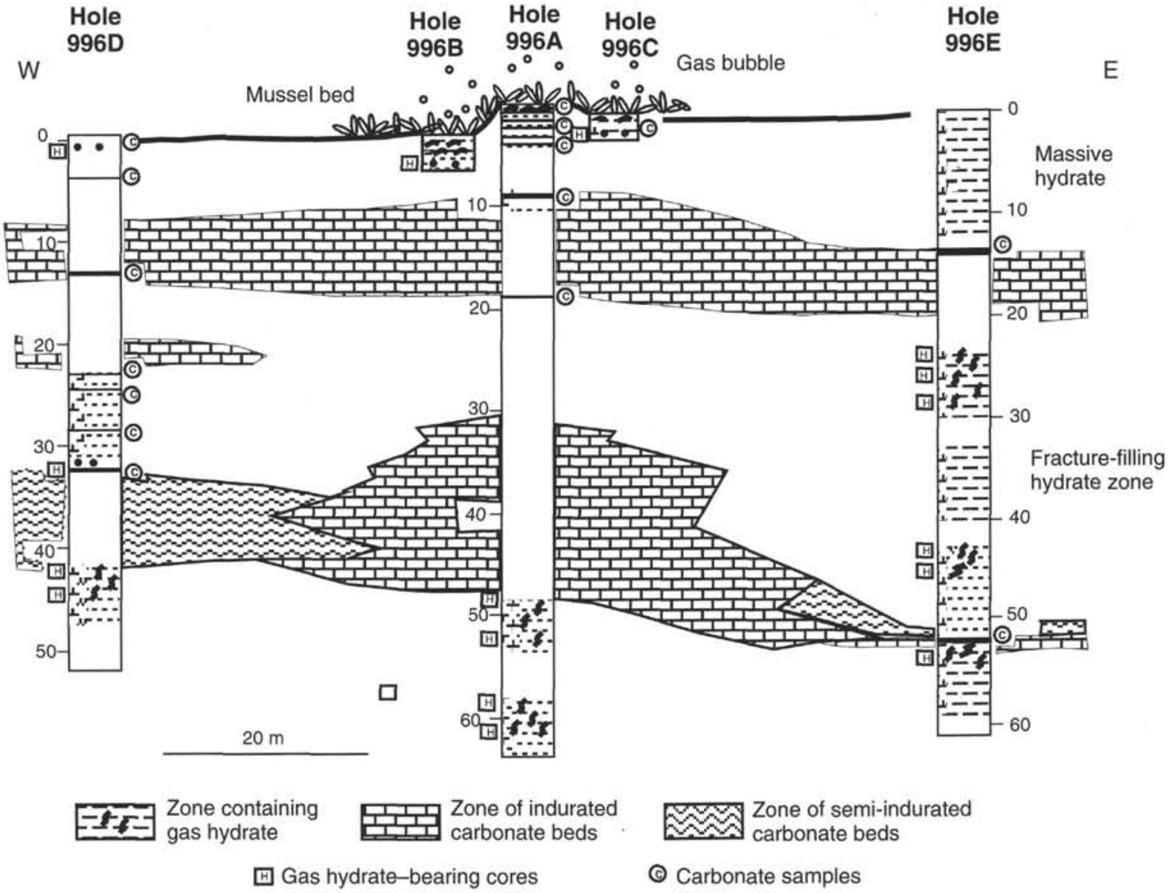

Figure 37. Schematic drawing showing the inferred distribution of authigenic carbonate zones and gas hydrate at Site 996. See the "Lithostratigraphy" section in the "Explanatory Notes" chapter (this volume) for an explanation of lithologic symbols. Each carbonate zone may be composed of several thinner beds. Interpretation of the vertical distribution of the carbonate beds relies on penetration-rate data to augment the core information. Holes 996A, 996B, and 996C are thought to be in the center of a pockmark; however, drill-pipe measurements indicate more complicated bathymetry.